A Robust Mixed-Integer Convex Model for Optimal Scheduling of Integrated Energy Storage – Soft Open Point Devices

Ilias Sarantakos, Meltem Peker, Natalia-Maria Zografou-Barredo, Matthew Deakin, *Member, IEEE*, Charalampos Patsios, *Member, IEEE*, Timur Sayfutdinov, Phil Taylor, *Senior Member, IEEE*, David Greenwood, *Member, IEEE*

***Abstract*—Soft open points (SOPs) are power electronic devices which can replace conventional normally open points in distribution networks. SOPs enable full control of active power flow between the interconnected feeders and can inject reactive power at each node to which they are connected. SOPs integrated with energy storage (ES) have been recently proposed to realize both spatial and temporal flexibility in active distribution networks. The flexibility provided by integrated ES-SOP devices will allow network operators to run their networks closer to their limits, but only if there is appropriate management of the uncertainty arising from demand and renewable generation. The only existing model of an ES-SOP uses nonconvex nonlinear equations, neglects uncertainty, and represents converter losses in an oversimplistic manner. This paper presents a robust mixed-integer convex model for the optimal scheduling of integrated ES-SOPs to ensure a zero probability of constraint violation. Losses of the subsystems comprising the ES-SOP are modelled using a proposed binary-polynomial model, enabling efficient scheduling of the energization state of subsystems to reduce no-load losses. The ES-SOP is considered in this paper to be owned by the network operator to: 1) manage power flow constraints, 2) minimize cost of losses, and 3) maximize arbitrage profit.**

***Index Terms*—Converter losses, convex optimization, energy storage, robust optimization, soft open point.**

NOMENCLATURE

A. Sets

D^t	Uncertainty set of nodal net injection at time t.
$k{:}j{\rightarrow}k$	Set of nodes connected to node j except node i.
Ω_b, Ω_n, Ω_t	Set of network branches / nodes / time periods.

B. Indices

i, j	Indices of nodes ($i, j \in \Omega_n$).
ij	Index of branch ij ($ij \in \Omega_b$).
t	Index of time.

C. Variables

$b_{1,t}$, $b_{2,t}$, $b_{3,t}$	Binary variables which define the energization state of AC-DC converters 1 and 2, and the DC-DC converter at time t.
$I_{ij,t}$	Current magnitude of branch ij, at time t.
$k_{11,t}$, $k_{12,t}$	Auxiliary variables for AC-DC converter 1.
$k_{21,t}$, $k_{22,t}$	Auxiliary variables for AC-DC converter 2.
$k_{3,t}$, $P^{\text{ES-SOP}}_{3,t\ \text{abs}}$	Auxiliary variables for the DC-DC converter.
$k_{4,t}$	Auxiliary variable for the battery.
$L_{ij,t}$	Squared current of branch ij at time t.
$P^{\text{ES-SOP}}_{1,t}$	Active power of AC-DC converter 1 at time t.
$P^{\text{ES-SOP,L}}_{1,t}$	Active power loss of AC-DC converter 1 at time t.
$P^{\text{ES-SOP}}_{2,t}$	Active power of AC-DC converter 2 at time t.
$P^{\text{ES-SOP,L}}_{2,t}$	Active power loss of AC-DC converter 2 at time t.
$P^{\text{ES-SOP}}_{3,t}$	Active power of the DC-DC converter at time t.
$P^{\text{ES-SOP,L}}_{3,t}$	Active power loss of the DC-DC converter at time t.
$P^{\text{ES-SOP}}_{4,t}$	Power output of the battery (positive for discharging) at time t.
$P^{\text{ES-SOP,L}}_{4,t}$	Battery power loss at time t.
$P_{ij,t}$, $Q_{ij,t}$	Active/Reactive power flow from node i to j, at time t.
$P^{\text{G}}_{i,t}$, $Q^{\text{G}}_{i,t}$	Active / Reactive power generation at node i, at time t.
$P^{\text{ES-SOP}}_{j,t}$	Active power injection by ES-SOP at node j, at time t.
$Q^{\text{ES-SOP}}_{1,t}$	Reactive power of AC-DC converter 1 at time t.
$Q^{\text{ES-SOP}}_{2,t}$	Reactive power of AC-DC converter 2 at time t.
$Q^{\text{ES-SOP}}_{j,t}$	Reactive power injection by ES-SOP at node j, time t.
$S^{\text{ES-SOP}}_{1,t}$	Apparent power of AC-DC converter 1 at time t.
$S^{\text{ES-SOP}}_{2,t}$	Apparent power of AC-DC converter 2 at time t.
SoC_t	State of charge of the battery at time t.
$V_{i,t}$, $u_{i,t}$	Voltage magnitude / Squared voltage at node i, time t.
θ	Binary variable used to define the uncertainty set.

D. Parameters

c_{a0}, c_{a1}, c_{a2}	AC-DC converter polynomial loss model coefficients.
c_{d0}, c_{d1}, c_{d2}	DC-DC converter polynomial loss model coefficients.
c_{aux}	Storage auxiliary / Battery management system losses.
c_{ES}	Storage internal resistance loss coefficient.
d^t_i	Uncertain net injection of node i at time t.
$\bar{d}^t_i$	Nominal value of the net injection of node i at time t.
$\hat{d}^t_i$	Deviation from the nominal net injection value.
$I_{ij,\max}$	Ampacity of branch ij.
$P^{\text{D}}_{i,t}$, $Q^{\text{D}}_{i,t}$	Active / Reactive power demand at node i, time t.
$P^{\text{ES}}_{\max}$	Power rating of energy storage / battery.
p_t	Day-ahead market price at time t.
R_{ij}, X_{ij}	Resistance / Reactance of branch ij.
$S^{\text{AC-DC}}_{\max}$	Rating of AC-DC converters.
$S^{\text{DC-DC}}_{\max}$	Rating of DC-DC converter.
T	Number of time periods.
$V_{\max}$, $V_{\min}$	Maximum and minimum voltage limit.
Δt	Duration of a single time period.

I. INTRODUCTION

SOFT OPEN POINTS (SOPs) are power electronic devices which provide a flexible interconnection (in terms of active power) between two or more feeders in electricity distribution networks [1]. The most common applications for which they have been studied are loss minimization (e.g. [2]) and power flow management (e.g. [3]). Energy storage (ES) systems can fulfil numerous functions in smart grids, including power flow management [4], and arbitrage [5]. However, multiple

This is the accepted version of an IEEE-copyrighted article, https://doi.org/10.1109/TSG.2022.3145709.

applications are often necessary to justify investment in ES systems [6].

Integrated energy storage – soft open point (ES-SOP) devices, which have been recently proposed in [7], offer a promising new solution which can provide both spatial (due to SOPs) and temporal (due to ES) flexibility to active distribution networks. This flexibility is offered at a reduced capital cost compared with installing an SOP and an ES system separately. This occurs as the SOP converters can be used to control charging/discharging of the ES, as shown in Fig. 1, without the need of additional converter(s) to interface the ES with two (or more) feeders of the network.

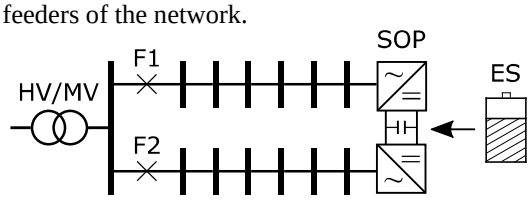

Fig. 1. An integrated ES-SOP device in a distribution network.

A. Applications of ES-SOPs in Distribution Networks

Power flow management can defer network reinforcement [4], and this will often be the primary motivation to install either an SOP or an ES to a distribution network. Power flow management is vulnerable to uncertainty because it involves managing the power flow in specific branches to ensure that violations of network limits do not occur in situations in which branch power flow will be very close to these limits. Distribution network operators (DNOs) are naturally conservative with respect to constraint violations – operating outside of acceptable limits is a danger to both life and property, and so ensuring sufficient robustness in the selected schedule of controllable devices, such as SOPs and ES systems, is of paramount importance.

Consequently, if an SOP or ES is scheduled neglecting uncertainty, it may lead to a high probability of a violation of technical constraints because even small perturbations in the demand or generation during peak load – given a predefined schedule – can cause the power flow to exceed its limits. This will be referred to as probability of constraint violation (PoCV).

This situation calls for suitable uncertainty management which ensures feasibility of the optimal schedule with a very high probability and without being overly conservative. A conservative schedule can result in a great headroom between the branch power flow and the corresponding limit, which indicates potential underutilization and opportunity cost for the ES system. Note that, in general, adding robustness increases the computational complexity. In general, nonconvex problems are NP-hard, and so can be very challenging to solve [8]. Ensuring that the formulation is convex is therefore paramount to ensure computational tractability.

Network loss reduction is a valuable objective which is most commonly considered in optimal SOP scheduling (e.g. [2]), and occasionally considered in ES scheduling (e.g. [9]). The regulatory framework around network losses is critical in this respect. Two types of incentives are used in the European countries investigated in [10]. The first, is an indicator introduced by the electricity regulator, e.g. a maximum acceptable threshold for network losses. The second (stricter) incentive, is that DNOs must buy energy at wholesale market price to compensate for losses. Both measures are applied to encourage network efficiency, encouraging DNOs to effectively manage losses within their networks.

This paper considers a system in which the second measure is used, and the focus is on optimal ES-SOP scheduling and its impact on the cost of losses (rather than simply network losses). The losses arising within the subsystems of the ES-SOP must be included in the overall cost of losses, and necessitate the inclusion of an appropriate ES-SOP loss model. The ES-SOP device consists of several naturally partitioned subsystems, and so there could be benefits of de-energizing individual subsystems if they have significant no-load losses (a practice which would be analogous to the idea of 'power gating' in VLSI design [11]). Such an approach leads to a substantial increase in the computational complexity, however, due to the introduction of binary variables. It is worthwhile noting that the losses in these converters are typically very significant – for example, in [12], it was found that power converters must be at least 97.8% efficient for it to be suitable for loss reduction in distribution networks. In other solid-state devices (e.g., solid state transformers), the device efficiency is also seen as a key challenge in device design [13].

Arbitrage takes advantage of the temporal variations in price to maximize profit [5]; this results in a schedule in which ES discharges when market price is high and charges when market price is low. This application has been widely used in the relevant literature with the aim of alleviating the impact of the significant capital cost of ES.

B. Uncertainty Management

The most prominent optimization methods capable of handling uncertainty are stochastic programming [14-16], chance-constrained optimization [17], and robust optimization [2, 18]. The first two require full knowledge of the probability distribution of the uncertain parameters, which might not be possible to acquire in practice. Moreover, stochastic programming easily becomes intractable as the number of scenarios rises, and chance-constrained optimization provides solutions with probabilistic guarantees, which might not be acceptable in all cases.

This paper uses (two-stage) robust optimization [18] because it: 1) does not require knowledge of the probability distribution of the uncertain parameters, 2) effectively controls the degree of conservatism, and 3) is computationally tractable (e.g. when used with cutting plane algorithms based on Benders decomposition or column and constraint generation [19]), provided underlying uncertainty sets satisfy some computability assumptions [20].

C. Scope of the Paper

This paper aims to create robust, day-ahead operational schedules for ES-SOP devices. These schedules could be used in conjunction with a real-time control stage which adapts the schedule to the realisation of uncertainty during operation, but this real-time control is not within the scope of this paper. Day-ahead scheduling is important because: 1) The inclusion of an ES system necessitates the advance scheduling of ES-SOP devices; otherwise, the energy resources of the ES may be depleted, resulting in either constraint violation or imbalance costs. 2) The schedule of these devices is required to be

optimized in advance, since the optimal schedule can inform the network operator for the procurement of network services, which should be contracted in advance [21].

D. Novelty and Contribution

This paper provides a method to optimize the schedule of a DNO-owned ES-SOP device, which manages power flow to ensure that network constraints are violated with zero probability (given that uncertainty realization lies within the predefined uncertainty set), whilst optimizing cost of losses and arbitrage profit attained through arbitrage.

Relevant literature [7] has provided an initial (nonconvex) model of integrated ES-SOP devices, which fails to address uncertainty, and models converter losses assuming constant efficiency. Therefore, the contributions of this work are:

1) We introduce a mixed-integer robust convex model for optimal scheduling of integrated ES-SOP devices. Two-stage adaptive robust optimization is employed to ensure a zero PoCV, while allowing adjustment of the conservatism of the solution. In the first stage, the ES-SOP schedule is decided, accounting for the worst-case uncertainty realization of demand and renewable generation, which is sought in the second stage within a predefined uncertainty set and for a given level of conservatism.
2) The losses of each subsystem in the ES-SOP device are modelled using a novel binary-polynomial model, with the binary variable modelling the energization state of each converter. This approach accurately captures the losses of each individual subsystem, even when individual converters are de-energized during idle periods. It is demonstrated that this discontinuous model leads to significant changes in the operating characteristics relative to models considered in previous works, with the turn-on losses suppressing low-power 'trickle transfer' between feeders and encourages ES charging/discharging through individual feeders to further limit total losses.
3) The proposed (initially nonconvex) ES-SOP binary-polynomial loss model is convexified to obtain a mixed-integer convex model.

Convexity in terms of continuous variables (as we have a mixed-integer convex problem [22]) is significant because it guarantees a computationally efficient and globally optimal solution by commercially available solvers [23].

The rest of the paper is organized as follows. Section II describes the ES-SOP loss model. Section III provides the problem formulation, introducing the deterministic problem, followed by the robust model. Then, Section IV outlines the solution methodology. Section V presents the case study, and simulation results are illustrated and discussed in Section VI. Finally, the conclusions are drawn in Section VII.

II. ES-SOP Losses

An integrated ES-SOP system has more subsystems than either an SOP or ES considered in isolation. As such, there are more opportunities to optimize the operation of individual subsystems of the device to reduce operational costs.

In this section we consider how the losses of individual subsystems can be modelled, with a particular focus on how no-load (energization) losses of converters can be effectively modelled and subsequently exploited to reduce operating costs. This is particularly valuable if an ES-SOP device is only operating at a fraction of its rated power.

A. Subsystem Modelling

A schematic of the system is presented in Fig. 2, and comprises of four subsystems: two AC-DC voltage source converters, a DC-DC interface converter, and the battery.

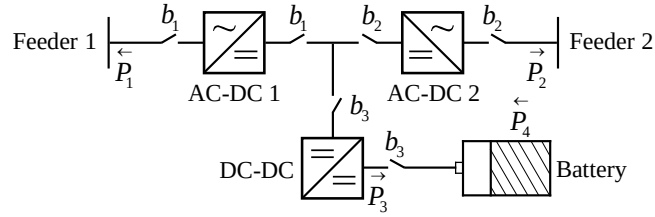

Fig. 2. Schematic of the ES-SOP device. The ES-SOP is composed of four subsystems: i) AC-DC converter 1, which connects the DC link with feeder 1, ii) AC-DC converter 2, which connects the DC link with feeder 2, 3) the DC-DC converter, which connects the DC link with the battery, and iv) the battery.

The losses for the AC-DC and DC-DC converters are modelled using a combination of a binary variable b, representing the on-off (energization) state of the device, and a second-order polynomial function of the apparent power S, which models the losses of the converter as the loading changes [24, 25]. The losses of the converter are therefore given by

$$P_{\text{Loss, Conv.}} = b\left(c_0 + c_1 S + c_2 S^2\right). \tag{1}$$

De-energizing a converter (i.e., setting $b = 0$) will result in zero losses, but the device can then no longer transfer active power or provide reactive support (so $S = 0$).

Whilst the values of (1) are assumed to be based on a regression-based approach, each of the polynomial loss coefficients c_0, c_1, c_2 can be attributed to different loss mechanisms within a converter. The constant voltage coefficient c_1 is due to switching losses and conduction losses in diode-like components, whilst the ohmic loss coefficient c_2 are due to ohmic conduction losses [26]. No-load energization losses c_0 are largely due to the no-load losses of passive components such as LCL filters and interface transformers [27-29]. Nevertheless, even with detailed physics-based modelling, not all converter losses can be attributed known physical mechanisms [25], further justifying the use of a model such as (1).

We consider a battery loss model of the form:

$$P_{\text{Loss, Batt.}} = c_{\text{aux}} + c_{\text{ES}} P^2, \tag{2}$$

where $P_{\text{Loss, Batt.}}$ are the losses in the battery, c_{aux} are auxiliary system losses, and the coefficient c_{ES} models losses due to the internal resistance of the battery. The losses above correspond to the low C-rate model, which best describes the battery operation patterns, considered in the present paper. Particularly, the considered battery applications, which include energy arbitrage and network losses reduction, implies that the battery C-rate does not exceed one [30]; for higher C-rate services, a more detailed battery loss model can be considered within the proposed framework.

The battery auxiliary losses c_{aux} are a result of safety-critical functions of a battery management system. Therefore, in contrast to losses in the converters c_0, we assume that the battery auxiliary system cannot be de-energized to reduce no-load

losses. For Li-ion battery chemistries, which are used in the majority of grid-scale ES systems, auxiliary losses can be assumed independent of system utilization [31].

1) Coefficient Values and System Efficiency

Table I lists the value of each coefficient used to model the subsystem losses of the ES-SOP device. The coefficients yield the power-efficiency curves shown in Fig. 3. The ES round-trip efficiency is calculated based on one charge-discharge cycle.

The curves show the models behave in a realistic manner: efficiency is very low at low powers, increasing quickly; peak efficiency is often at part-load, with a reduction at high powers as conduction losses increase [32, 33]. Likewise, the round-trip, full-load ES efficiency between 85% and 90% is close to values attained in real utility-scale systems [34].

TABLE I
ES-SOP SUBSYSTEM LOSS COEFFICIENT VALUES FOR LOSS MODELS (1), (2)

Symbol	c_{a0}	c_{a1}	c_{a2}	c_{d0}	c_{d1}	c_{d2}	c_{aux}	c_{ES}
Value (% of rated power)	0.5	0.5	2	0.35	0.25	1.4	0.2	1.6

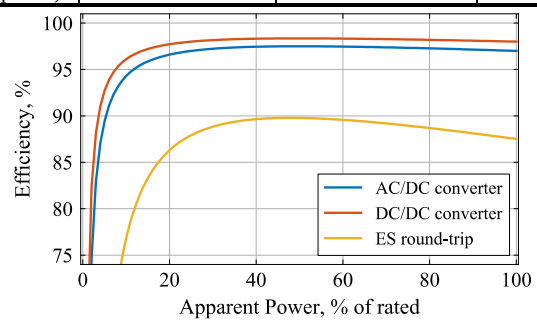

Fig. 3. Efficiency as a function of power for the AC-DC converter, the DC-DC converter, and total round-trip efficiency of the ES system, using loss models (1), (2), and coefficients as in Table I.

B. Converter and Storage Loss Model

This section provides equations that describe the losses of: 1) AC-DC converters; 2) the DC-DC converter; and 3) the battery.

1) AC-DC Converters

Equations (3) and (4) describe the losses of the two AC-DC converters which connect the DC link on the one side with the endpoints of feeders 1 and 2 of the network on the other.

$$P_{1,t}^{\text{ES-SOP,L}} = b_{1,t}\left(c_{a0} + c_{a1}S_{1,t}^{\text{ES-SOP}} + c_{a2}\left(S_{1,t}^{\text{ES-SOP}}\right)^2\right) \tag{3}$$

$$P_{2,t}^{\text{ES-SOP,L}} = b_{2,t}\left(c_{a0} + c_{a1}S_{2,t}^{\text{ES-SOP}} + c_{a2}\left(S_{2,t}^{\text{ES-SOP}}\right)^2\right) \tag{4}$$

which can be written as:

$$P_{1,t}^{\text{ES-SOP,L}} = c_{a0}b_{1,t} + c_{a1}k_{11,t} + c_{a2}k_{12,t} \tag{5}$$

$$P_{2,t}^{\text{ES-SOP,L}} = c_{a0}b_{2,t} + c_{a1}k_{21,t} + c_{a2}k_{22,t} \tag{6}$$

which are linear constraints.

In (5) and (6), auxiliary (nonnegative) variables $k_{11,t}$, $k_{12,t}$, $k_{21,t}$, $k_{22,t}$ are defined as follows:

$$\begin{aligned} k_{11,t} &= S_{1,t}^{\text{ES-SOP}} = \sqrt{\left(P_{1,t}^{\text{ES-SOP}}\right)^2 + \left(Q_{1,t}^{\text{ES-SOP}}\right)^2} \Leftrightarrow \\ k_{11,t}^2 &= \left(P_{1,t}^{\text{ES-SOP}}\right)^2 + \left(Q_{1,t}^{\text{ES-SOP}}\right)^2 \end{aligned} \tag{7}$$

$$k_{12,t} = \left(S_{1,t}^{\text{ES-SOP}}\right)^2 = \left(P_{1,t}^{\text{ES-SOP}}\right)^2 + \left(Q_{1,t}^{\text{ES-SOP}}\right)^2 \tag{8}$$

$$\begin{aligned} k_{21,t} &= S_{2,t}^{\text{ES-SOP}} = \sqrt{\left(P_{2,t}^{\text{ES-SOP}}\right)^2 + \left(Q_{2,t}^{\text{ES-SOP}}\right)^2} \Leftrightarrow \\ k_{21,t}^2 &= \left(P_{2,t}^{\text{ES-SOP}}\right)^2 + \left(Q_{2,t}^{\text{ES-SOP}}\right)^2 \end{aligned} \tag{9}$$

$$k_{22,t} = \left(S_{2,t}^{\text{ES-SOP}}\right)^2 = \left(P_{2,t}^{\text{ES-SOP}}\right)^2 + \left(Q_{2,t}^{\text{ES-SOP}}\right)^2 \tag{10}$$

which are relaxed, and written as the following second-order cone constraints:

$$\left\| P_{1,t}^{\text{ES-SOP}} \quad Q_{1,t}^{\text{ES-SOP}} \right\|_2 \le k_{11,t} \tag{11}$$

$$\left\| 2P_{1,t}^{\text{ES-SOP}} \quad 2Q_{1,t}^{\text{ES-SOP}} \quad 1 - k_{12,t} \right\|_2 \le 1 + k_{12,t} \tag{12}$$

$$\left\| P_{2,t}^{\text{ES-SOP}} \quad Q_{2,t}^{\text{ES-SOP}} \right\|_2 \le k_{21,t} \tag{13}$$

$$\left\| 2P_{2,t}^{\text{ES-SOP}} \quad 2Q_{2,t}^{\text{ES-SOP}} \quad 1 - k_{22,t} \right\|_2 \le 1 + k_{22,t} \tag{14}$$

The exactness (i.e. relaxed constraints are binding at optimality) is guaranteed by the objective function, which minimizes cost of losses, and is presented in Section III-A. The proof can be found in Appendix A. A detailed explanation for the derivation of (12) and (14) can be found in Appendix B.

The following constraints ensure that when binary variables $b_{1,t}$, $b_{2,t}$ are zero, then $P_{1,t}^{\text{ES-SOP,L}}, P_{2,t}^{\text{ES-SOP,L}}$ are also zero.

$$k_{11,t} \le b_{1,t} S_{\max}^{\text{AC-DC}} \tag{15}$$

$$k_{12,t} \le b_{1,t}\left(S_{\max}^{\text{AC-DC}}\right)^2 \tag{16}$$

$$k_{21,t} \le b_{2,t} S_{\max}^{\text{AC-DC}} \tag{17}$$

$$k_{22,t} \le b_{2,t}\left(S_{\max}^{\text{AC-DC}}\right)^2 \tag{18}$$

2) DC-DC Converter

Equation (19) gives the losses of the DC/DC converter, which connects the DC link with the battery.

$$P_{3,t}^{\text{ES-SOP,L}} = b_{3,t}\left(c_{d0} + c_{d1}\left|P_{3,t}^{\text{ES-SOP}}\right| + c_{d2}\left(P_{3,t}^{\text{ES-SOP}}\right)^2\right) \tag{19}$$

which can be written as:

$$P_{3,t}^{\text{ES-SOP,L}} = c_{d0}b_{3,t} + c_{d1}P_{3,t\,\text{abs}}^{\text{ES-SOP}} + c_{d2}k_{3,t} \tag{20}$$

which is a linear constraint.

Auxiliary variables $P_{3,t\,\text{abs}}^{\text{ES-SOP}}, k_{3,t}$ in (20) are defined below:

$$P_{3,t\,\text{abs}}^{\text{ES-SOP}} = \left|P_{3,t}^{\text{ES-SOP}}\right| \tag{21}$$

$$k_{3,t} = \left(P_{3,t}^{\text{ES-SOP}}\right)^2 \tag{22}$$

Equation (21) is linearized as follows:

$$P_{3,t\,\text{abs}}^{\text{ES-SOP}} \ge P_{3,t}^{\text{ES-SOP}}, \quad P_{3,t\,\text{abs}}^{\text{ES-SOP}} \ge -P_{3,t}^{\text{ES-SOP}} \tag{23}$$

Equation (22) is relaxed, and written as the following second-order cone constraint:

$$\left\| 2P_{3,t}^{\text{ES-SOP}} \quad 1 - k_{3,t} \right\|_2 \le 1 + k_{3,t} \tag{24}$$

To make sure that when binary variable $b_{3,t}$ is zero, then $P_{\text{L}3,t}$ is also zero, we introduce the following constraints:

$$P_{3,t\,\text{abs}}^{\text{ES-SOP}} \le b_{3,t} S_{\max}^{\text{DC-DC}} \tag{25}$$

$$k_{3,t} \le b_{3,t}\left(S_{\max}^{\text{DC-DC}}\right)^2 \tag{26}$$

3) Battery

Equation (27) describes battery losses:

$$P_{4,t}^{\text{ES-SOP,L}} = c_{\text{aux}} + c_{\text{ES}}\left(P_{4,t}^{\text{ES-SOP}}\right)^2 \tag{27}$$

which can be written as the following linear constraint:

$$P_{4,t}^{\text{ES-SOP,L}} = c_{\text{aux}} + c_{\text{ES}} k_{4,t} \tag{28}$$

where

$$k_{4,t} = \left(P_{4,t}^{\text{ES-SOP}}\right)^2 \tag{29}$$

Equality (29) is relaxed to a second-order cone constraint:

$$\left\| 2P_{4,t}^{\text{ES-SOP}} \quad 1 - k_{4,t} \right\|_2 \le 1 + k_{4,t} \tag{30}$$

III. Problem Formulation

A. Deterministic Problem

This section presents the deterministic model: 1) the objective function, 2) the constraints, and 3) the full model.

1) Objective function

We consider a single objective function, expressed in monetary terms, which comprises the cost of losses of the ES-SOP device, the arbitrage profit, and the cost of network losses:

$$\min \sum_{t \in \Omega_t} \left[\begin{array}{l} \underbrace{\left(P_{1,t}^{\text{ES-SOP,L}} + P_{2,t}^{\text{ES-SOP,L}} + P_{3,t}^{\text{ES-SOP,L}} + P_{4,t}^{\text{ES-SOP,L}}\right) p_t \Delta t}_{\text{ES-SOP Loss Cost}} \\ \underbrace{-P_{4,t}^{\text{ES-SOP}} p_t \Delta t}_{\text{Arbitrage Profit}} + \underbrace{\left(\sum_{ij \in \Omega_b} R_{ij} I_{ij,t}^2\right) p_t \Delta t}_{\text{Cost of Network Losses}} \end{array} \right] \tag{31}$$

2) Constraints

a) Power Flow Constraints

Power flow constraints are formulated according to *DistFlow branch equations* [35, 36] employing the convex relaxation in [37, 38]. Relaxation gaps are evaluated in Section VI to provide information for the quality of the solution, as in [39]. A graphical representation of the power flow equations employed in this paper is shown in Fig. 4. The equations are presented below (for each time period) [37]. Defining variables $u_{i,t}$ and $L_{ij,t}$, as squared voltage and squared current, respectively, facilitates the convex formulation of the power flow model.

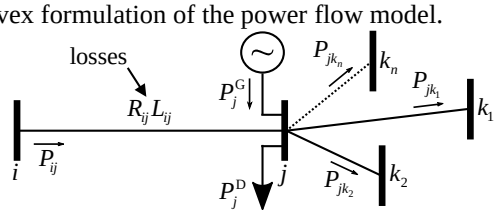

Fig. 4. Graphical representation of the *DistFlow branch equations*. The active (and reactive) power flow at the sending node of branch *ij* equals the sum of: i) sum of power flows from node *j* to nodes $k_1, k_2, \ldots, k_n$, ii) branch losses, iii) demand at node *j*, and iv) minus generation at node *j* [39].

$$P_{ij,t} = \sum_{k: j \to k} P_{jk,t} + R_{ij} L_{ij,t} + P_{j,t}^{\text{D}} - P_{j,t}^{\text{G}}, \ \forall\ ij \in \Omega_b \tag{32}$$

$$Q_{ij,t} = \sum_{k: j \to k} Q_{jk,t} + X_{ij} L_{ij,t} + Q_{j,t}^{\text{D}} - Q_{j,t}^{\text{G}}, \ \forall\ ij \in \Omega_b \tag{33}$$

$$u_{j,t} = u_{i,t} - 2\left(R_{ij} P_{ij,t} + X_{ij} Q_{ij,t}\right) + \left(R_{ij}^2 + X_{ij}^2\right) L_{ij,t}, \ \forall\ ij \in \Omega_b \tag{34}$$

where

$$u_{i,t} = V_{i,t}^2, \ \forall\ i \in \Omega_n \tag{35}$$

$$L_{ij,t} = \left(P_{ij,t}^2 + Q_{ij,t}^2\right) \Big/ u_{i,t} = I_{ij,t}^2, \ \forall\ ij \in \Omega_b \tag{36}$$

which is relaxed to [37, 38]:

$$\left\| 2P_{ij,t} \quad 2Q_{ij,t} \quad L_{ij,t} - u_{i,t} \right\|_2 \le L_{ij,t} + u_{i,t} \tag{37}$$

Integrating the ES-SOP device into the network, (32) and (33) become:

$$P_{ij,t} - \sum_{k: j \to k} P_{jk,t} - R_{ij} L_{ij,t} = P_{j,t}^{\text{D}} - P_{j,t}^{\text{G}} - \underbrace{P_{j,t}^{\text{ES-SOP}}}_{\text{if ES-SOP at node } j}, \ \forall\ ij \in \Omega_b \tag{38}$$

$$Q_{ij,t} - \sum_{k: j \to k} Q_{jk,t} - X_{ij} L_{ij,t} = Q_{j,t}^{D} - Q_{j,t}^{G} - \underbrace{Q_{j,t}^{\text{ES-SOP}}}_{\text{ES-SOP at node } j}, \ \forall\ ij \in \Omega_b \tag{39}$$

Network operational constraints are as follows:

$$V_{\min}^2 \le u_{i,t} \le V_{\max}^2, \ \forall\ i \in \Omega_n \tag{40}$$

$$L_{ij,t} \le I_{ij,\max}^2, \ \forall ij \in \Omega_b \tag{41}$$

b) ES-SOP Constraints

This section presents the rest of the equations that govern the operation of the ES-SOP device. Converter and storage loss equations have already been given in Section II-B. Therefore, the rest of the ES-SOP model is detailed below:

$$SoC_{t+1} = SoC_t - \left(P_{4,t}^{\text{ES-SOP}} + P_{4,t}^{\text{ES-SOP,L}}\right) \Delta t \tag{42}$$

$$-P_{\max}^{\text{ES}} \le P_{4,t}^{\text{ES-SOP}} \le P_{\max}^{\text{ES}} \tag{43}$$

$$SoC_{\min} \le SoC_t \le SoC_{\max} \tag{44}$$

$$SoC_1 = SoC_T \tag{45}$$

Equation (42) represents how the state of charge (SoC) of the battery changes based on the power of the device and its losses. Equations (43) and (44) impose limits on the power and energy of the battery, and (45) ensures that the SoC at the beginning of the day is equal to the SoC at the end of the day. Power balance constraints for the ES-SOP device, as shown in Fig. 2, are given by (46) and (47).

$$P_{3,t}^{\text{ES-SOP}} = -\left(P_{4,t}^{\text{ES-SOP}} - P_{4,t}^{\text{ES-SOP,L}}\right) \tag{46}$$

$$P_{1,t}^{\text{ES-SOP}} + P_{2,t}^{\text{ES-SOP}} + P_{3,t}^{\text{ES-SOP}} + P_{1,t}^{\text{ES-SOP,L}} + P_{2,t}^{\text{ES-SOP,L}} + P_{3,t}^{\text{ES-SOP,L}} = 0 \tag{47}$$

Finally, capacity constraints for AC-DC converter 1, AC-DC converter 2, and the DC-DC converter are represented by (48), (49), and (50), respectively.

$$\sqrt{\left(P_{1,t}^{\text{ES-SOP}}\right)^2 + \left(Q_{1,t}^{\text{ES-SOP}}\right)^2} \le S_{\max}^{\text{AC-DC}} \Leftrightarrow \left\| P_{1,t}^{\text{ES-SOP}} \quad Q_{1,t}^{\text{ES-SOP}} \right\|_2 \le S_{\max}^{\text{AC-DC}} \tag{48}$$

$$\left\| P_{2,t}^{\text{ES-SOP}} \quad Q_{2,t}^{\text{ES-SOP}} \right\|_2 \le S_{\max}^{\text{AC-DC}} \tag{49}$$

$$-S_{\max}^{\text{DC-DC}} \le P_{3,t}^{\text{ES-SOP}} \le S_{\max}^{\text{DC-DC}} \tag{50}$$

3) Model

The decision variables of the optimization problem are: $u_{i,t}$, $P_{ij,t}$, $Q_{ij,t}$, $L_{ij,t}$, $P_{1,t}^{\text{ES-SOP}}$, $P_{1,t}^{\text{ES-SOP,L}}$, $P_{2,t}^{\text{ES-SOP}}$, $P_{2,t}^{\text{ES-SOP,L}}$, $P_{3,t}^{\text{ES-SOP}}$, $P_{3,t}^{\text{ES-SOP,L}}$, $P_{4,t}^{\text{ES-SOP}}$, $P_{4,t}^{\text{ES-SOP,L}}$, $Q_{1,t}^{\text{ES-SOP}}$, $Q_{2,t}^{\text{ES-SOP}}$, $k_{11,t}$, $k_{12,t}$, $k_{21,t}$, $k_{22,t}$, $P_{3,t\ \text{abs}}^{\text{ES-SOP}}$, $k_{3,t}$, $k_{4,t}$, SoC_t, $b_{1,t}$, $b_{2,t}$, $b_{3,t}$. The full model is shown below:

minimize (31)

subject to (5), (6), (11)-(18), (20), (23)-(26),

(28), (30), (34), (37)-(50)

B. Compact Form of the Deterministic Model

This section presents the deterministic model in a compact form, which are referred to in explanations of the robust model and solution methodology in sections III.C and IV, respectively.

$$\min \ \mathbf{c}^{\mathrm{T}}\mathbf{x}+\mathbf{e}^{\mathrm{T}}\mathbf{y} \tag{51}$$

$$\text{s.t.} \quad \mathbf{Ax} \le \mathbf{b} \tag{52}$$

$$\left\|\mathbf{Fx}\right\|_2 \le \mathbf{f}^{\mathrm{T}}\mathbf{x} \tag{53}$$

$$\mathbf{Hx}+\mathbf{Ky}=\mathbf{d} \tag{54}$$

$$\mathbf{My} \le \mathbf{r} \tag{55}$$

$$\left\|\mathbf{Gy}\right\|_2 \le \mathbf{g}^{\mathrm{T}}\mathbf{y} \tag{56}$$

where **x** is the vector of first stage decision variables, which are all ES-SOP scheduling variables, and **y** is the vector of second stage decision variables, which corresponds to power flow variables $u_{i,t}$, $P_{ij,t}$, $Q_{ij,t}$, $L_{ij,t}$. Note that the separation of variables and constraints in two stages (in this section) takes place to make a smoother transition to the two-stage adaptive robust model. In the objective function (51), the first term represents the ES-SOP loss cost minus arbitrage profit (first and second term in (31)), while the second term represents the cost of network losses (third term in (31)). Constraint (52) collects first stage, linear constraints (5), (6), (15)-(18), (20), (23), (25), (26) , (42)-(47), and (50). Constraint (53) represents first stage, second-order cone constraints (11)-(14), (24), (30), (48), and (49). Constraint (54) denotes second stage, linear equality constraints (active and reactive power balance for each branch) (38), (39), for which uncertainty will be considered (demand and renewable generation). Constraint (55) collects the rest of second stage linear constraints (34), (40), and (41). Finally, constraint (56) corresponds to second stage, second-order cone constraint (37).

C. Robust Model

The inherent uncertainty of demand and renewable generation is addressed in this paper using two-stage adaptive robust optimization [18], which ensures a feasible solution for given uncertainty intervals. In the first stage, ES-SOP schedule is determined taking into account all possible uncertainty realizations. The resulting schedule is feasible, thus robust, for any uncertainty realization of demand and renewable generation. In the second stage, the worst-case scenario, for which maximum feeder loading occurs (which can lead to constraint violation), is sought within a predefined uncertainty set. We subsequently present the uncertainty set and the two-stage adaptive robust model.

1) Uncertainty Set

We combine the uncertainty of demand and renewable generation, and we therefore consider nodal net injection, as an uncertain parameter, with the following uncertainty set at each time period [18, 40]:

$$D^t\left(\overline{\mathbf{d}}^t,\hat{\mathbf{d}}^t,\Gamma^t\right):=\left\{\begin{array}{l}\mathbf{d}^t \in \mathbb{R}^{|\Omega_n|}: \sum_{i\in\Omega_n}\left(\theta_{i,t}^{+}+\theta_{i,t}^{-}\right)\le \Gamma^t, \theta_{i,t}^{+}+\theta_{i,t}^{-}\le 1, \\ d_i^t=\overline{d}_i^t+\hat{d}_i^t\theta_{i,t}^{+}-\hat{d}_i^t\theta_{i,t}^{-},\ \forall i\in\Omega_n\end{array}\right\} \tag{57}$$

Based on (57), d_i^t takes values within the following interval:

$$d_i^t \in \left[\overline{d}_i^t-\hat{d}_i^t, \overline{d}_i^t+\hat{d}_i^t\right] \tag{58}$$

A user-defined parameter, which is called budget of uncertainty (Γ^t), adjusts the level of robustness/conservatism of the solution. A zero value for the budget of uncertainty corresponds to the deterministic case and will result in an unacceptably high probability of constraint violation (PoCV), especially if the network is operated close to its limits. Conversely, if the budget of uncertainty takes its maximum value (which is equal to the number of nodes of the network), it ensures that there is a feasible solution for all possible realizations within the uncertainty interval. This (fully robust) solution corresponds to a zero PoCV but is overconservative, resulting in a higher operational cost. The level of conservatism is adjusted to ensure a zero PoCV, without requiring a significant sacrifice in terms of objective function value.

2) Two-Stage Adaptive Robust Model

Having described the uncertainty set D^t, we present the two-stage adaptive robust model, in compact form, below:

$$\begin{array}{l}\min\limits_{\mathbf{x}} \ \left(\mathbf{c}^{\mathrm{T}}\mathbf{x}+\max\limits_{\mathbf{d}\in D}\ \min\limits_{\mathbf{y}\in\Omega(\mathbf{x},\mathbf{d})}\ \mathbf{e}^{\mathrm{T}}\mathbf{y}\right) \\ \text{s.t.} \quad \mathbf{Ax}\le\mathbf{b},\ \left\|\mathbf{Fx}\right\|_2\le\mathbf{f}^{\mathrm{T}}\mathbf{x}\end{array} \tag{59}$$

where

$$\Omega\left(\mathbf{x},\mathbf{d}\right)=\left\{\mathbf{y}:\mathbf{Hx}+\mathbf{Ky}=\mathbf{d},\ \mathbf{My}\le\mathbf{r},\ \left\|\mathbf{Gy}\right\|_2\le\mathbf{g}^{\mathrm{T}}\mathbf{y}\right\} \tag{60}$$

is the set of feasible power flow solutions for a fixed ES-SOP schedule **x** and nodal net injections **d**. Second stage variables **y** are adjustable (i.e. tune themselves) to each uncertainty realization **d**, and given ES-SOP schedule **x**.

The separation of variables has been implemented in the following way. First stage variables include the actual decisions that the operator must make, i.e., ES-SOP scheduling variables. These decisions are made before uncertainty is revealed. Power flow variables ($u_{i,t}$, $P_{ij,t}$, $Q_{ij,t}$, $L_{ij,t}$) are indeed decision variables, but they do not represent actual decisions. They are adjustable variables that adjust themselves to each uncertainty realization (i.e., after uncertainty has been revealed) and ES-SOP power injections to feeders. Therefore, power flow variables are classified as second stage variables.

IV. Solution Methodology

The proposed two-stage adaptive robust model (59), (60) is initially a tri-level min-max-min problem, which is eventually converted to a bilevel problem (shown later) that cannot be directly solved by commercial software, and requires a specific solution approach. By taking the dual of the inner minimization, we first merge the second and third level problems and obtain a two-level problem. We then decompose the resulting model to solve the robust problem, for which different cutting plane algorithms have been proposed in the literature, as it cannot be directly solved by off-the-shelf solvers.

Benders decomposition [41, 42] iteratively introduces constraints (cuts) to the model using dual solutions of the second-stage problem. Column and constraint generation (CCG) [19] creates constraints and new variables for the worst-case uncertainty realization at each iteration. In [19], it is shown that CCG provides tighter bounds for the objective function, which reduces the number of iterations. This is why CCG has been chosen in this paper to solve our two-stage model. In CCG method, the problem is decomposed into a master problem (MP) and a subproblem (SP), which are solved iteratively. The MP provides a lower bound for the original problem and at each iteration by adding cuts to the MP, which are derived from the

optimal solution of the SP, it provides better lower bounds. The algorithm continues until the lower bound from the MP and the upper bound from the SP converge. In Section IV-A, we provide the MP and the SP using the compact form (59), (60).

In the robust model, we use the budget of uncertainty (Γ^t), which adjusts the level of robustness. For a fixed first stage decision vector ($\mathbf{x}^*$), the problem reduces to determining the worst-case realization of nodal net injection $\mathbf{d}$. For an integer Γ^t, it is shown that the worst-case realization occurs when uncertain nodal net injections are either at the upper or lower limits of the uncertainty set [43]. Thus, the optimal solution of the reduced model occurs at an extreme point of the uncertainty set. If we denote all extreme points of uncertainty set, the reduced model can be equivalently written as a model with a large but finite number of constraints. However, solving the formulation with all extreme points is impractical for many problems. Nevertheless, one can easily observe that solving the formulation with a subset of extreme points provides a lower bound for the original problem. Therefore, a CCG algorithm that adds constraints for one extreme point at each iteration provides stronger lower bounds at each iteration and it will terminate in a finite number of iterations with an optimal solution.

A. Master Problem (MP)

The MP determines the ES-SOP schedule and satisfies the constraints for the scenarios added so far. For the mth iteration of the algorithm, the MP is given below:

$$f_{\text{m}} = \min\ \mathbf{c}^{\text{T}}\mathbf{x} + \eta \tag{61}$$

$$\text{s.t.}\quad \mathbf{Ax} \le \mathbf{b} \tag{62}$$

$$\left\|\mathbf{Fx}\right\|_2 \le \mathbf{f}^{\text{T}}\mathbf{x} \tag{63}$$

$$\eta \ge \mathbf{e}^{\text{T}}\mathbf{y}^v,\ \forall v = 1,\ldots,m \tag{64}$$

$$\mathbf{Hx} + \mathbf{Ky}^v = \mathbf{d}^v,\ \forall v = 1,\ldots,m \tag{65}$$

$$\mathbf{My}^v \le \mathbf{r},\ \forall v = 1,\ldots,m \tag{66}$$

$$\left\|\mathbf{Gy}^v\right\|_2 \le \mathbf{g}^{\text{T}}\mathbf{y}^v,\ \forall v = 1,\ldots,m \tag{67}$$

where v (= 1,…,m) corresponds to iterations that have been performed so far (i.e. v is associated with the variables and constraints added up to the mth iteration), and η is the auxiliary variable that minimizes the second stage objective function value. At each iteration, new variables $\mathbf{y}^m$ are introduced, and new constraints (64)-(67) are added to the MP, which are derived from the optimal solution of the SP. $\mathbf{d}^v$ is obtained from the solution of the SP, and $\mathbf{y}^v$ are the corresponding second stage decision variables.

B.Subproblem (SP)

For a given first stage decision vector $\mathbf{x}^*$, which represents the ES-SOP schedule, the following subproblem determines the worst-case realization of nodal net injection $\mathbf{d}$.

$$\max_{\mathbf{d}\in D}\ \min_{\mathbf{y}\in\Omega(\mathbf{x},\mathbf{d})}\ \mathbf{e}^{\text{T}}\mathbf{y} \tag{68}$$

$$\text{s.t.}\quad \mathbf{Hx}^* + \mathbf{Ky} = \mathbf{d}\quad (\boldsymbol{\lambda}) \tag{69}$$

$$\mathbf{My} \le \mathbf{r}\quad (\boldsymbol{\pi}) \tag{70}$$

$$\left\|\mathbf{Gy}\right\|_2 \le \mathbf{g}^{\text{T}}\mathbf{y}\quad (\boldsymbol{\omega},\boldsymbol{\varphi}) \tag{71}$$

where $\boldsymbol{\lambda}$, $\boldsymbol{\pi}$, $\boldsymbol{\omega}$, and $\boldsymbol{\varphi}$ are the corresponding dual decision variables. To solve the SP, we first transform the bilevel model into a single-level model making use of conic duality theory [44], which results in the following bilinear model.

$$\max_{\mathbf{d},\boldsymbol{\pi},\boldsymbol{\lambda},\boldsymbol{\omega},\boldsymbol{\varphi}}\ \left(\mathbf{d} - \mathbf{Hx}^*\right)\boldsymbol{\lambda} + \mathbf{r}\boldsymbol{\pi} \tag{72}$$

$$s.t.\quad \mathbf{K}\boldsymbol{\lambda} + \mathbf{M}\boldsymbol{\pi} + \sum_{h=1}^{H}\left(\mathbf{G}\boldsymbol{\omega} + \mathbf{g}\boldsymbol{\varphi}\right) = \mathbf{e} \tag{73}$$

$$\left\|\boldsymbol{\omega}\right\|_2 \le \boldsymbol{\varphi} \tag{74}$$

$$\boldsymbol{\lambda}\ \text{free},\ \boldsymbol{\pi} \le 0,\ \boldsymbol{\omega}\ \text{free},\ \boldsymbol{\varphi} \ge 0 \tag{75}$$

where H is the number of constraints in (71).

The proposed model remains exact in our robust optimization framework since second-order cones (71) are self-dual, which means that they appear as second-order cones (74) in the dual model [45]. Furthermore, in the solution approach explained below, for a fixed first stage decision vector ($\mathbf{x}^*$), since the primal SP satisfies Slater's condition, strong duality holds; and by strong duality theorem of second-order cone programming problems [44], the primal SP and dual SP attain the same objective function values.

The bilinear term $\mathbf{d}\boldsymbol{\lambda}$ in the objective function can be linearized since the feasible regions of the bilinear term are bounded and disjoint. For an integer Γ^{t}, there exists an optimal solution at an extreme point of the uncertainty set; and at the optimal solution, θ^+ and θ^- take a value of either 0 or 1. Hence, bilinear terms can be linearized using the Big-M method and the above problem can then be reformulated as a mixed-integer second-order cone programming problem.

$$f_{\text{s}} = \max_{\sigma^+,\sigma^-,\theta^+,\theta^-,\lambda,\pi,\omega,\varphi}\ \bar{\mathbf{d}}\boldsymbol{\lambda} + \hat{\mathbf{d}}\boldsymbol{\sigma}^+ - \hat{\mathbf{d}}\boldsymbol{\sigma}^- - \mathbf{Hx}^*\boldsymbol{\lambda} + \mathbf{r}\boldsymbol{\pi} \tag{76}$$

$$s.t.\quad \mathbf{K}\boldsymbol{\lambda} + \mathbf{M}\boldsymbol{\pi} + \sum_{h=1}^{H}\left(\mathbf{G}\boldsymbol{\omega} + \mathbf{g}\boldsymbol{\varphi}\right) = \mathbf{e} \tag{77}$$

$$\left\|\boldsymbol{\omega}\right\|_2 \le \boldsymbol{\varphi} \tag{78}$$

$$-M^+_{ij,t}\theta^+_{ij,t} \le \sigma^+_{ij,t} \le M^+_{ij,t}\theta^+_{ij,t},\ \forall ij \in \Omega_{\text{b}},\ \forall t \in \Omega_{\text{t}} \tag{79}$$

$$-M^+_{ij,t}\left(1-\theta^+_{ij,t}\right) + \lambda_{ij,t} \le \sigma^+_{ij,t} \le \lambda_{ij,t} + M^+_{ij,t}\left(1-\theta^+_{ij,t}\right) \tag{80}$$

$$-M^-_{ij,t}\theta^-_{ij,t} \le \sigma^-_{ij,t} \le M^-_{ij,t}\theta^-_{ij,t},\ \forall ij \in \Omega_{\text{b}},\ \forall t \in \Omega_{\text{t}} \tag{81}$$

$$-M^-_{ij,t}\left(1-\theta^-_{ij,t}\right) + \lambda_{ij,t} \le \sigma^-_{ij,t} \le \lambda_{ij,t} + M^-_{ij,t}\left(1-\theta^-_{ij,t}\right) \tag{82}$$

$$\boldsymbol{\lambda}\ \text{free},\ \boldsymbol{\pi} \le 0,\ \boldsymbol{\omega}\ \text{free},\ \boldsymbol{\varphi} \ge 0,\ \boldsymbol{\sigma}^+,\boldsymbol{\sigma}^-\ \text{free},\ \boldsymbol{\theta}^+,\boldsymbol{\theta}^- \in \{0,1\} \tag{83}$$

where $M_{ij,t}$ are sufficiently large numbers, and $\sigma_{ij,t}^+ = \lambda_{ij,t}\theta_{ij,t}^+$, $\sigma_{ij,t}^- = \lambda_{ij,t}\theta_{ij,t}^-$, which are linearized by constraints (79)-(82). For instance, constraints (79) and (80) reduce to $\sigma_{ij,t}^+ = \lambda_{ij,t}$, if $\theta_{ij,t}^+ = 1$, and $\sigma_{ij,t}^+ = 0$, if $\theta_{ij,t}^+ = 0$. Algorithm 1 provides the procedure of the described solution methodology.

Algorithm 1: Column and Constraint Generation

1. Set LB = -∞, UB = +∞, m = 0, tolerance ε.
2. **while** (UB - LB < ε) **do**
3. Solve the MP (61)-(67). Get optimal solution and objective, $\mathbf{x}^*$ and f_{m}, respectively. LB ← max{LB, f_{m} }.
4. Given $\mathbf{x}^*$, solve the dual SP (76)-(83). Get worst-case uncertainty realization $\mathbf{d}^*$ and objective f_{s}. UB ← min{UB, $\mathbf{c}^{\text{T}}\mathbf{x}^* + f_{\text{s}}$ }.
5. $\mathbf{d}^{\text{m+1}}$ ← $\mathbf{d}^*$. Introduce new variables $\mathbf{y}^{\text{m+1}}$. Add constraints (64)-(67) to the MP.
6. $m \leftarrow m + 1$.
7. **end**
8. Return $\mathbf{x}^*$.

V. Case Study

A. Test Network and Input Data

The test network is composed of two IEEE 33-bus systems connected via an ES-SOP as shown in Fig. 5. Each converter is rated at 400 kVA, and the battery is 400 kW / 800 kWh. The ES-SOP manages feeder power flows – with a limit of 3.45 MVA – while optimizing cost of losses and arbitrage profit. Customer types are shown in Table II, and the corresponding load profiles are taken from [46]. The location and capacity of distributed generation is shown in Fig. 5; the associated profiles are from the North-East of England, in 2019, and were produced using [47]. The day-ahead market price profile is taken from [48], and is shown in Fig. 6. The simulation is run for 24 hours and input data correspond to a typical winter weekday.

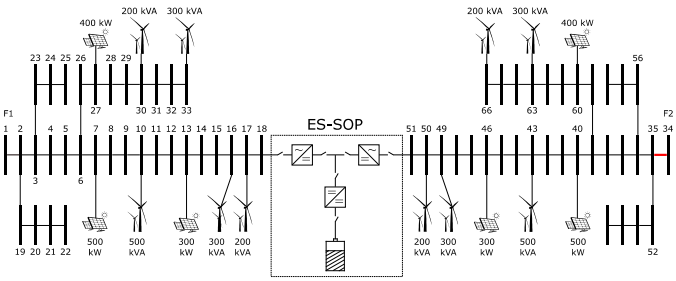

Fig. 5. The case study network showing the location and capacity of distributed generation and ES-SOP. Constrained branch is shown in red.

TABLE II
Customer Types for the Test Network

Customer Type	Load Points (Buses)
Residential	2-6, 9-13, 15-22, 26-28, 33, 35-56, 59-64
Commercial	7-8, 14, 23, 29-32, 65-65
Industrial	24-25, 57-58

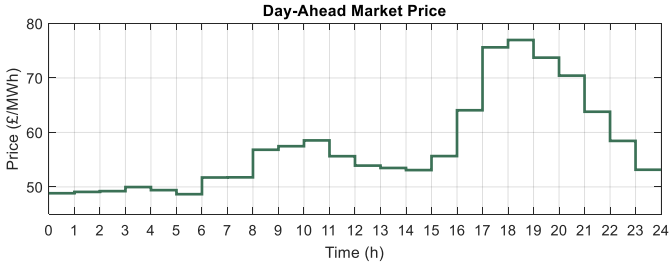

Fig. 6. Day-ahead market price.

VI. Results and Discussion

The proposed methodology was applied to the network shown in Fig. 5, using the data described in Section V. The model was formulated in MATLAB R2017a using YALMIP [49] and optimized using Gurobi [50]. An Intel Core i7 octa-core processor at 3.00 GHz with 32 GB of RAM was used for the simulations. Optimality gap was set to 0.5%. The following subsections demonstrate: A) the impact of the ES-SOP loss model; B) the accuracy of the proposed model with respect to the convex relaxations; C) the impact of uncertainty; D) a comparison with two-stage stochastic programming; and E) the application of the proposed model to a real-world distribution network.

A. ES-SOP Loss Model

This section compares the ES-SOP schedules produced by the proposed model and [7], which is considered as a benchmark. The constant-efficiency assumption of [7] for ES and SOP devices is common in previous works considering each of those systems in isolation [2, 51]. The deterministic model described in section III-A is used for comparison with [7], because the focus is on the ES-SOP loss model. Fig. 7 shows the loading of each feeder considering optimal ES-SOP operation; the network is heavily loaded, and the margin between maximum feeder demand and the line limit is small.

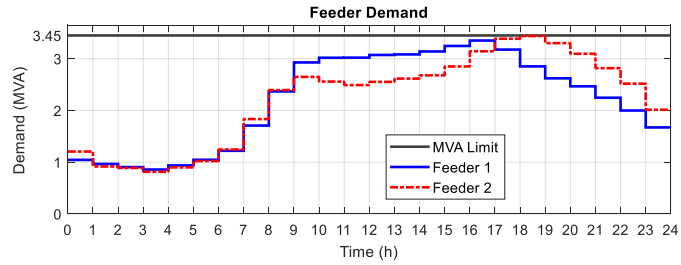

Fig. 7. Feeder demand considering optimal ES-SOP operation – deterministic model. The network is heavily loaded; the margin between maximum demand and feeder capacity is very small.

Fig. 8 presents the optimal ES-SOP schedules generated by our proposed model and [7]. Both profiles demonstrate the spatial and temporal flexibility provided by an ES-SOP.

During periods of significant mismatch in feeder load, the ES-SOP device acts in a SOP-like mode, transferring power between feeders. This relieves the network with the higher demand, thereby reducing total system losses and managing active thermal constraints (which occurs when feeder demand is equal to the thermal limit of the line). An example of this spatial flexibility is demonstrated in Fig. 8a-c from 11:00 – 12:00, 15:00 – 17:00, and 20:00 – 22:00. During these periods, ES power is zero but the active power injections to the feeders are nonzero, indicating a load transfer between the feeders to reduce network losses. In all cases, demand is effectively moved from the heavily to the lightly loaded feeder. Because the demand on the two profiles follow different profiles, the direction of this transfer changes throughout the day.

As well as shifting energy in space, the ES-SOP device can, via the ES system, provide temporal flexibility by shifting demand in time. In Fig. 8c, the ES discharges and injects to both feeders between 17:00 and 20:00, when price is at its highest. Because the demand on feeder 2 is higher than that of feeder 1 (at these time periods), more active power is injected to the former (see Fig. 8a-b). This demonstrates spatial flexibility in these time periods as well, which can be considered as a superimposition of these two characteristics.

We now examine the impact of considering the proposed ES-SOP loss model against the benchmark model [7], by comparing their output. The proposed model considers the capability of a converter to be de-energized in order to save costs incurred by no-load losses. This is evident in Fig. 8a-b during 01:00 – 02:00 and 20:00 – 23:00. In the first time interval, the proposed model increases the utilization of AC-DC converter 1 to compensate the de-energization of AC-DC converter 2. During the second time interval, the utilization of both AC-DC converters is increased (between 20:00 – 22:00) due to the reduced marginal losses at low powers for the proposed model. Conversely, between 22:00 – 23:00, the low power 'trickle transfer' is suppressed, as the real power transfer is too small to overcome the no-load losses. As such, AC-DC converter 1 switches off (Fig. 8d).

The benchmark [7] considers a linear loss model for all subsystems, which results in constant efficiency. Conversely, our proposed model considers a quadratic term for losses, which results in drop in efficiency at high powers. This penalizes utilization close to the rated power (0.4 MVA) of the converters and storage, as shown in Fig. 8c-e.

When the ES-SOP device is switched on (i.e., if all binary switches *b* are enabled), the marginal cost of losses increases with power, so small powers have the lowest marginal losses. As a result, and because the device is already energized to provide support to the feeders (see Fig. 8a-c), the ES-SOP device can take advantage of the smaller price differential from mid-morning to mid-afternoon.

The above observations are quantified in Table III, which presents the differences between the two models for each subsystem of the objective function and the saving compared to the operation without the ES-SOP device. This (no ES-SOP operation) is associated with an overall cost of £162.7 (per day), of network losses only, as there is neither ES-SOP loss cost, nor arbitrage profit. The ES-SOP schedule produced by the benchmark model is also evaluated using our proposed loss model and is shown in bold (in Table III). The benchmark model underestimates ES-SOP loss cost by 13.4%. The proposed model generates an 8% higher arbitrage profit, and results in an overall saving 21.4% greater than that of the benchmark model.

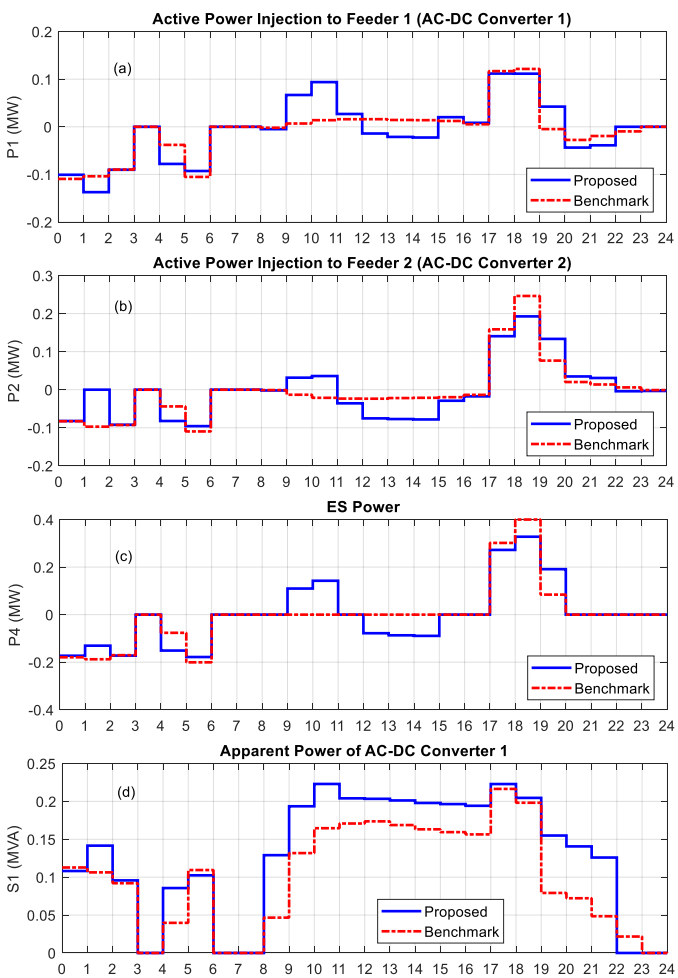

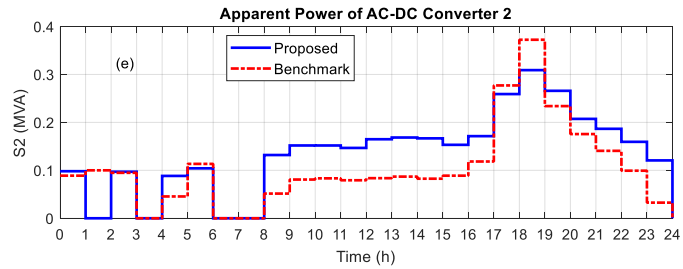

Fig. 8. ES-SOP optimal schedules produced by our proposed model (solid blue lines) and the benchmark [7] (dash-dotted red lines).

TABLE III
COMPARISON OF OUR PROPOSED MODEL WITH BENCHMARK [7]

	Proposed Model	Benchmark [7]	Difference (%)
Network Loss Cost (£)	145.8	148.1	-
ES-SOP Loss Cost (£)	14.6	12.9 (**14.9**)	-
Arbitrage Profit (£)	-21.5	-19.9	-
Total (£)	138.9	141.1 (**143.1**)	-
Saving (£)	23.8	21.6 (**19.6**)	+21.4%

B. Evaluation of Relaxation Gaps

This section evaluates the relaxation gaps for the constraints that have been relaxed. Relatively small gap values indicate that the relaxations are practical for the model [39, 52]. Five gaps are defined as follows:

$$Gap_{1,t} = \left| P_{1,t}^{\text{ES-SOP,L}} - b_{1,t}\left(c_{a0} + c_{a1}S_{1,t}^{\text{ES-SOP}} + c_{a2}\left(S_{1,t}^{\text{ES-SOP}}\right)^2\right)\right| \quad (84)$$

$$Gap_{2,t} = \left| P_{2,t}^{\text{ES-SOP,L}} - b_{2,t}\left(c_{a0} + c_{a1}S_{2,t}^{\text{ES-SOP}} + c_{a2}\left(S_{2,t}^{\text{ES-SOP}}\right)^2\right)\right| \quad (85)$$

$$Gap_{3,t} = \left| P_{3,t}^{\text{ES-SOP,L}} - b_{3,t}\left(c_{d0} + c_{d1}\left|P_{3,t}^{\text{ES-SOP}}\right| + c_{d2}\left(P_{3,t}^{\text{ES-SOP}}\right)^2\right)\right| \quad (86)$$

$$Gap_{4,t} = \left| P_{4,t}^{\text{ES-SOP,L}} - \left(c_{\text{aux}} + c_{\text{ES}}\left(P_{4,t}^{\text{ES-SOP}}\right)^2\right)\right| \quad (87)$$

$$Gap_{5,ij,t} = \left| \sqrt{L_{ij,t}} - \sqrt{\left(P_{ij,t}^2 + Q_{ij,t}^2\right)/u_{i,t}}\right| \quad (88)$$

which are associated with the original (i.e. prior to relaxation) constraints (3), (4), (19), (27), and (36), respectively. The mean values of these gaps are presented in Table IV, along with the mean values of $P_{1,t}^{\text{ES-SOP,L}}, P_{2,t}^{\text{ES-SOP,L}}, P_{3,t}^{\text{ES-SOP,L}}, P_{4,t}^{\text{ES-SOP,L}}, \sqrt{L_{ij,t}}$.

TABLE IV
RELAXATION GAPS

Relaxation Gap	Mean Value	Variable	Mean Value	Relative Gap
Gap_1 (MW)	7.81×10^{-9}	$P_{1,t}^{\text{ES-SOP,L}}$ (MW)	0.0034	$2.30\text{x}10^{-5}$
Gap_2 (MW)	8.74×10^{-9}	$P_{2,t}^{\text{ES-SOP,L}}$ (MW)	0.0036	$2.43\text{x}10^{-5}$
Gap_3 (MW)	2.05×10^{-9}	$P_{3,t}^{\text{ES-SOP,L}}$ (MW)	0.0016	$1.28\text{x}10^{-5}$
Gap_4 (MW)	1.26×10^{-9}	$P_{4,t}^{\text{ES-SOP,L}}$ (MW)	0.0015	$8.40\text{x}10^{-6}$
Gap_5 (A)	2.27×10^{-4}	$L_{ij,t}^{0.5}$ (A)	26.06	$8.71\text{x}10^{-5}$

Comparing each relaxation gap with the corresponding variable, we can notice a difference of 5-6 orders of magnitude, which indicates satisfactory accuracy of the proposed model.

C. Impact of Uncertainty

1) Deterministic Model

The deterministic model neglects uncertainty of the input data and optimizes the model assuming the uncertain parameters will take their base case values. This assumption means that feasibility of the optimal solution can only be guaranteed for that specific case. To demonstrate this, the feasibility of the ES-SOP schedule obtained from the deterministic model has been examined by running 100 Monte Carlo simulations to explore different realizations of the uncertainty. This is carried out in the following way: the ES-SOP schedule is considered fixed, which we use to run a power flow for each (time step of each) day, varying the uncertain parameter (i.e. nodal net injection) at each iteration, by sampling from its uncertainty set (±10% [51]). Uniform distribution is used for nodal net injection, as the corresponding uncertainty set for robust optimization is the interval shown in (58).

Fig. 9 shows that 43.1% of the simulated days leads to violations of the capacity constraint at branch 34-35 (Feeder 2). The optimal ES-SOP schedule for the nominal values of the uncertain parameters gives a branch loading, which is below the associated limit by only a tiny margin, as illustrated in Fig. 7. This results in a high rate of constraint violation in the Monte Carlo simulation, as even a slight increase in net demand during peak load can cause branch loading to violate its thermal limit. This issue is addressed in this study by using robust optimization, which immunizes the solution against uncertainty (given that data perturbation lies within the considered limits) to a predefined level of conservatism set by the decision-maker.

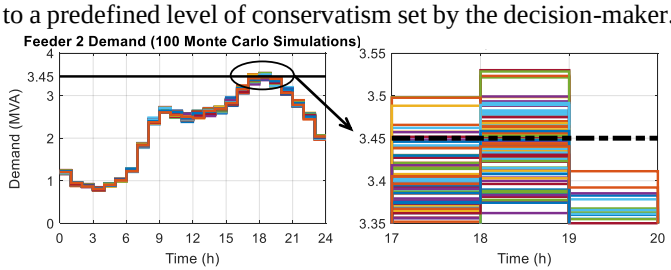

Fig. 9. Monte Carlo simulations to examine the feasibility of the ES-SOP schedule obtained by the deterministic model; 43.1% of simulated days led to constraint violation. Black line corresponds to branch capacity limit.

2) Robust Model

The infeasibility shown in Section VI-C1 provides the motivation to use robust optimization. This section provides results from the robust model for different levels of conservatism and finds the budget of uncertainty (Γ^t) which ensures zero PoCV with the minimum increase in the objective function value.

Table V shows the robust optimal value and the PoCV (calculated by 1,000 Monte Carlo simulations) for each Γ^t. Note that the robust optimal value is equal to the objective function value for the worst-case realization (for a given budget of uncertainty). Therefore, we also calculate the mean value of the objective function across all uncertainty realizations yielded by the Monte Carlo simulations. In this study, Γ^t ranges between zero and number of nodes (here 64 with nonzero load), with zero corresponding to the deterministic case and maximum value to fully robust; a value of 10 for Γ^t corresponds to the worst combination of 10 load points (for each time step) with maximum deviation from their nominal value. We can see in Table V that in order to get a robust solution that guarantees a zero PoCV, we need to pay a price, which is the increase in cost; this is the so-called *price of robustness* [53]. The required computational time for the proposed two-stage adaptive robust model was 68s.

TABLE V
POCV, ROBUST OPTIMAL VALUE, AND MEAN OBJECTIVE FUNCTION VALUE FOR DIFFERENT VALUES OF Γ

Γ^t	PoCV	Rob. Opt. Value	Increase	Mean Obj. Fun. Value	Increase
0	43.1%	£138.95	0%	-	-
3	17.6%	£142.87	2.8%	£139.15	0.14%
6	3.8%	£146.16	5.2%	£139.18	0.17%
9	0.3%	£149.22	7.4%	£139.53	0.42%
10	0%	£150.17	8.1%	£139.76	0.58%

Fig. 10 compares the quality of deterministic and robust (Γ^t = 10) solutions in terms of constraint violation, using Monte Carlo simulation. This figure demonstrates the effectiveness of robust optimization, which can reduce the PoCV to zero with only an 8.1% increase in cost in the worst case, and only 0.58% on average.

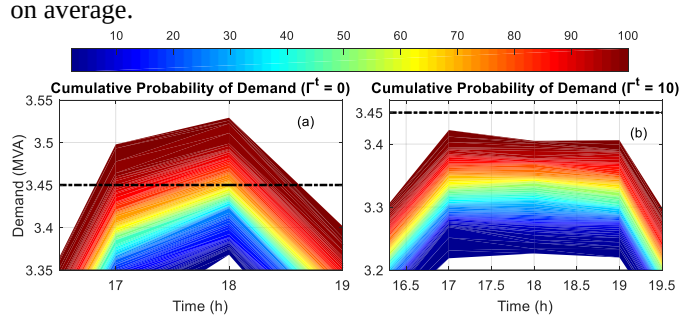

Fig. 10. Cumulative probability of feeder 2 demand from 100 Monte Carlo simulations for deterministic and robust solutions. In (a), Γ^t = 0, i.e. deterministic model – PoCV = 43.1%; and in (b), Γ^t = 10 – PoCV = 0%.

Fig. 11 compares the ES-SOP schedules derived by the deterministic and robust (Γ^t = 10) models. The active power injected to feeder 2 is increased by 32% at time 18:00, when there was the highest probability of violation in the deterministic case (see Fig. 9). Overall, +25% more energy (during 17:00 – 19:00) is injected to feeder 2 to mitigate the probability of violation compared to the deterministic case. Concurrently, the injection to feeder 1 is considerably lower (during 17:00 – 19:00), which means that the available energy in the battery is mainly used to relieve feeder 2, which is very close to its limit during this period, rather than inject to feeder 1, which has a greater margin (see Fig. 7).

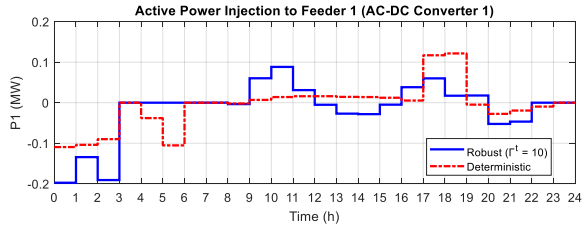

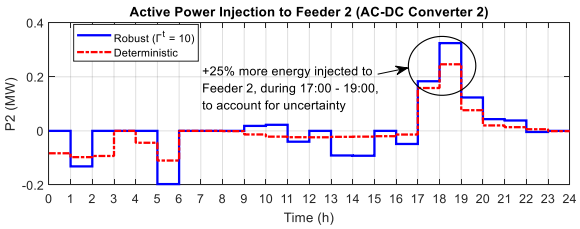

Fig. 11 ES-SOP schedules (active power injections to feeders) determined by: deterministic model (dash-dotted red lines), and robust model using Γ^t = 10 (solid blue lines).

D. Comparison with Two-Stage Stochastic Programming

This section compares the proposed model with two-stage stochastic programming, which was formulated based on [14, 15]. The separation of variables between stages remains the same. The second stage variables are now scenario-dependent. Scenarios have been created using Monte Carlo simulation for the uncertain parameters. The results are summarized in Tables VI and VII.

Table VI shows that the stochastic programming model cannot reach an optimality gap of 0.5% (which was the one set for the robust model) within an hour, even for two scenarios. For ten scenarios, the model was not able to produce a feasible solution within two hours. This can be justified, however, by the complexity of the deterministic (mixed-integer) model, and the increasingly high computational burden, as number of scenarios rises.

Table VII presents results for the stochastic programming model when optimality gap is set to 3%; 20 runs of the model have been carried out. The average PoCV decreases when number of scenarios increases, as feasibility is ensured in more cases this way. However, both average PoCV and the PoCV range are not acceptable, and considerably more scenarios are needed. But, for ten scenarios, no feasible solution was found within two hours. Therefore, the use of stochastic programming is not suitable for this model.

TABLE VI
RESULTS OF TWO-STAGE STOCHASTIC PROGRAMMING I
(OPTIMALITY GAP = 0.5%)

Number of Scenarios	Computational Time	Optimality Gap
2	1h	>2%
5	1h	>2.5%
10	No feasible solution found in 2h	
Robust	68s	0.5%

TABLE VII
RESULTS OF TWO-STAGE STOCHASTIC PROGRAMMING II
(OPTIMALITY GAP = 3%)

Number of Scenarios	Average PoCV	PoCV Range
2	31.55%	9%-66%
5	24.07%	11%-53%
10	N/A	N/A

E. Application to a Real-World Distribution Network

This section presents an application of our model to a real-world system, which has been used in several papers and technical reports (e.g. [54, 55]). This is a real 11 kV urban network from the North-East of England, comprising seven feeders, of which two have been chosen for this study (feeders A1 and A3 from [54, 55]). These two feeders are illustrated in Fig. 12, and the corresponding data are given in [56]. The location and capacity of distributed generation is shown in Fig. 12; the associated profiles are from the North-East of England, in 2019, and have been produced using [47]. Each converter is rated at 400 kVA, and the battery is 400 kW / 1 MWh. Feeder limit is 2 MVA.

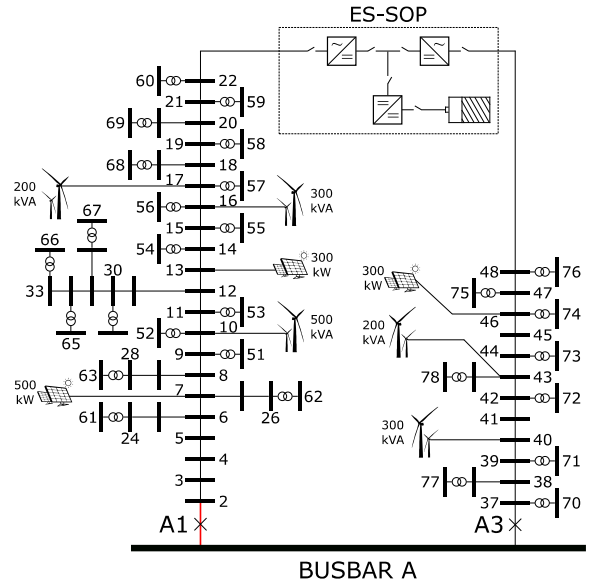

Fig. 12. A real-world distribution network from the North-East of England.

1) Impact of ES-SOP Loss Model

This subsection compares the results obtained by our deterministic model and the benchmark [7], which are shown in Table VIII. Operation without the ES-SOP device corresponds to a total cost of £66.68 (per day), of network losses only. The saving for our model is 83.7% greater than the benchmark (for the real-world distribution network), which can be justified by the low percentage (26%) of time that converters are energized. This is, in turn, justified by the lighter loading compared to the first test network (Section VI-A), as illustrated in Fig. 13. The corresponding percentage for the first test network was 72%. The fact that converters are off for so many time steps (for the real-world distribution network) allows such a big difference to occur. The benchmark model underestimates ES-SOP loss cost by 40% in this case. The ES-SOP loss cost difference between the proposed model and the benchmark is approximately £6/day, and is the main contributor to the overall saving difference of 83.7%. Given that the reduction in operational costs is a key component in the justification for SOPs and ES systems [57], this represents a significant improvement in performance.

TABLE VIII
COMPARISON OF OUR PROPOSED MODEL WITH BENCHMARK [7] – REAL-WORLD DISTRIBUTION NETWORK

	Proposed Model	Benchmark [7]	Difference (%)
Network Loss Cost (£)	69.37	69.38	-
ES-SOP Loss Cost (£)	8.06	8.49 (**14.14**)	-
Arbitrage Profit (£)	-25.28	-24.75	-
Total (£)	52.15	53.12 (**58.77**)	-
Saving (£)	14.53	13.56 (**7.91**)	+83.7%

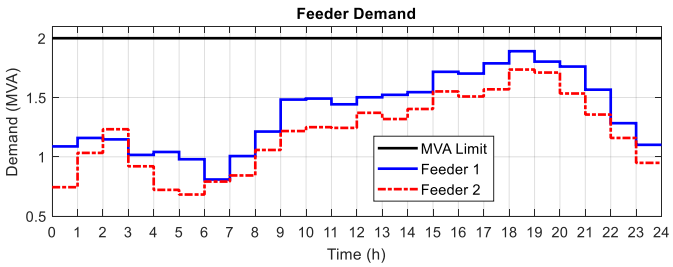

Fig. 13. Feeder demand considering optimal ES-SOP operation – deterministic model – real-world distribution network. The network is heavily loaded (but not so much as in the first test case); the margin between maximum demand and feeder capacity is small.

2) Impact of Uncertainty

This subsection shows how our model manages uncertainty in the real-world distribution network in terms of PoCV. In this case, we considered an energy storage with greater energy capacity (1 MWh instead of 800 kWh, as in the first test case); for this reason, we increased the uncertainty to 15%. The results of the robust model are shown in Table IX. We can see that the real-world distribution network is not so heavily loaded as the first test network because of the much lower PoCV for $\Gamma^t = 0$. Our model has been successfully applied to this network resulting in zero PoCV (for $\Gamma^t = 3$) with an increase in the average total cost of approximately 1% and 14.5% in the worst case.

TABLE IX
POCV, ROBUST OPTIMAL VALUE, AND MEAN OBJECTIVE FUNCTION VALUE FOR DIFFERENT VALUES OF Γ – REAL-WORLD DISTRIBUTION NETWORK

Γ^t	PoCV	Rob. Opt. Value	Increase	Mean Obj. Fun. Value	Increase
0	8%	£52.15	0%	-	-
1	3.6%	£55.33	6.1%	£52.22	0.13%
2	1.5%	£56.98	9.3%	£52.40	0.47%
3	0%	£59.73	14.5%	£52.69	1.03%

VII. CONCLUSION

This paper has introduced a robust mixed-integer convex model for the optimal scheduling of Energy Storage-Soft Open Point (ES-SOP) devices in distribution networks. ES-SOPs are integrated devices which can provide both spatial and temporal flexibility to network operators. However, their business case can rely on fulfilling multiple applications in uncertain conditions, requiring a method to maximize the value of the device in scenarios with variable demand and generation.

Existing ES-SOP models represented the losses of the whole device using constant efficiency (linear loss term). This paper introduced a binary-polynomial model which quantifies the non-linear relationship between device losses and utilization and enables explicit modelling of converter de-energization to reduce no-load losses during idle periods. Results from a real network in the North East of England show these considerations have a significant impact (40% ES-SOP loss cost underestimation by the benchmark model) on the losses incurred within the device, and substantially change the optimal device schedule (83.7% greater saving than that of the benchmark model).

The optimal schedules created using deterministic optimization methods resulted in an unacceptably high probability of network constraint violation: this is because the network was operated close to its limits and any unforeseen increase in net demand could lead to specific branches being overloaded. A two-stage adaptive robust optimization was used to address this issue; the probability of constraints being violated (given the assumed uncertainty set) could be reduced to zero with only a 1.03% increase in the average operating cost of the network (14.5% increase in the worst case). If a small but non-zero probability of constraint violation is acceptable to the operator, the method allows them to decrease the budget of uncertainty to decrease the operating cost in exchange for a low but acceptable probability of violating network limits.

In this paper, the ES-SOP was assumed to be owned and operated by the DNO. In future work, the implications of this assumption could be further explored. Alternative ownership models and business cases could be investigated to assess which ownership models deliver the best value for energy customers while ensuring sufficient incentive for investment in ES-SOPs.

APPENDIX A
EXACTNESS OF THE ES-SOP LOSS MODEL RELAXATIONS

This appendix provides a proof for the exactness of ES-SOP loss model relaxations, i.e. the relaxations of (7)-(10), (22), and (29). To facilitate the understanding of the proof, we expand the objective function (31), omitting p_t and Δt, which are positive, and are multiplied by all terms in (89).

$$\min \sum_{t\in\Omega_t} \left[\begin{array}{l} \underbrace{\left(c_{a0}b_{1,t} + c_{a1}k_{11,t} + c_{a2}k_{12,t}\right)}_{P_{1,t}^{\text{ES-SOP,L}}} + \underbrace{\left(c_{a0}b_{2,t} + c_{a1}k_{21,t} + c_{a2}k_{22,t}\right)}_{P_{2,t}^{\text{ES-SOP,L}}} \\ + \underbrace{\left(c_{d0}b_{3,t} + c_{d1}P_{3,t\ \text{abs}}^{\text{ES-SOP}} + c_{d2}k_{3,t}\right)}_{P_{3,t}^{\text{ES-SOP,L}}} + \underbrace{\left(c_{\text{aux}} + c_{\text{ES}}k_{4,t}\right)}_{P_{4,t}^{\text{ES-SOP,L}}} \\ -P_{4,t}^{\text{ES-SOP}} + \sum_{ij\in\Omega_b} R_{ij,t} I_{ij,t}^2 \end{array} \right] \tag{89}$$

Proposition: The relaxations of constraints (7)-(10), (22), (29) are exact.

Proof: We show exactness of the relaxed model (see Section III-A3) for constraint (29), and a similar approach can be followed for the other relaxations. Assume that there exists an optimal solution

$$w^* = \left(\ldots, k_{4,t}^*, P_{4,t}^{\text{ES-SOP}^*}, P_{4,t}^{\text{ES-SOP,L}^*}, \ldots\right) \tag{90}$$

of the relaxed model, and constraint (30) is not binding at w^*, i.e.

$$\left\| 2P_{4,t}^{\text{ES-SOP}} \quad 1-k_{4,t} \right\|_2 < 1+k_{4,t} \tag{91}$$

or, equivalently,

$$\left(P_{4,t}^{\text{ES-SOP}^*}\right)^2 < k_{4,t}^* \tag{92}$$

For some small enough $\varepsilon > 0$, there exists another solution of the relaxed model, w', where w' is equal to w^* except $k_{4,t}^*, P_{4,t}^{\text{ES-SOP}^*}, P_{4,t}^{\text{ES-SOP,L}^*}$, i.e.

$$w' = \left(\ldots, k_{4,t}', P_{4,t}^{\text{ES-SOP}'}, P_{4,t}^{\text{ES-SOP,L}'}, \ldots\right) \tag{93}$$

such that

$$k_{4,t}' = k_{4,t}^* - \varepsilon \tag{94}$$

$$P_{4,t}^{\text{ES-SOP}'} = P_{4,t}^{\text{ES-SOP}^*} - c_{\text{ES}}\varepsilon \tag{95}$$

$$P_{4,t}^{\text{ES-SOP,L}'} = P_{4,t}^{\text{ES-SOP,L}^*} - c_{\text{ES}}\varepsilon \tag{96}$$

We next show that w' is a feasible solution, and it has the same objective function value as w^*. Note that the changes (i.e. (94)-(96)) only affect constraints (28), (30), and (46) of the relaxed model. By substituting (94)-(96) into (28), (30), (46), it can be verified that w' satisfies these constraints, and thus w' is also a feasible solution of the relaxed model.

Then, by substituting (94)-(96) into the objective function, we observe that w' has the same objective function value as w^*, which shows that the relaxed model has alternative optimal solutions. Since the feasible region of the relaxed model is bounded, we can deduce that there exists an $\varepsilon > 0$, for which constraints (94)-(96) are satisfied and constraint (30) is binding. Therefore, we can conclude that we can find an exact optimal solution with the same objective function value as w^*. ■

Note that the above proof is similar to the relaxation exactness proof provided in [37].

Appendix B
Derivation of Relaxed Constraints (12) and (14)

Constraint (8) is relaxed to:

$$k_{12,t} \geq \left(P_{1,t}^{\text{ES-SOP}}\right)^2 + \left(Q_{1,t}^{\text{ES-SOP}}\right)^2 \tag{97}$$

which can be rearranged as follows:

$$\begin{aligned} &4\left(P_{1,t}^{\text{ES-SOP}}\right)^2 + 4\left(Q_{1,t}^{\text{ES-SOP}}\right)^2 - 4k_{12,t} \leq 0 \Leftrightarrow \\ &\left(2P_{1,t}^{\text{ES-SOP}}\right)^2 + \left(2Q_{1,t}^{\text{ES-SOP}}\right)^2 + \left(1-k_{12,t}\right)^2 - \left(1+k_{12,t}\right)^2 \leq 0 \Leftrightarrow \\ &\left(2P_{1,t}^{\text{ES-SOP}}\right)^2 + \left(2Q_{1,t}^{\text{ES-SOP}}\right)^2 + \left(1-k_{12,t}\right)^2 \leq \left(1+k_{12,t}\right)^2 \end{aligned} \tag{98}$$

which can be written as the following second-order cone constraint, which is identical to constraint (12).

$$\left\| 2P_{1,t}^{\text{ES-SOP}} \quad 2Q_{1,t}^{\text{ES-SOP}} \quad 1-k_{12,t} \right\|_2 \leq 1+k_{12,t} \tag{99}$$

A similar approach can be followed for the conversion of constraint (10) to constraint (14).

References

[1] E. Romero-Ramos, A. Gómez-Expósito, A. Marano-Marcolini, J. M. Maza-Ortega, and J. L. Martinez-Ramos, "Assessing the loadability of active distribution networks in the presence of DC controllable links," *IET Gener. Transm. Distrib.*, vol. 5, no. 11, pp. 1105-1113, 2011, doi: 10.1049/iet-gtd.2011.0080.

[2] H. Ji, C. Wang, P. Li, F. Ding, and J. Wu, "Robust Operation of Soft Open Points in Active Distribution Networks With High Penetration of Photovoltaic Integration," *IEEE Trans. Sustain. Energy*, vol. 10, no. 1, pp. 280-289, 2019, doi: 10.1109/TSTE.2018.2833545.

[3] Q. Qi, C. Long, J. Wu, and J. Yu, "Impacts of a medium voltage direct current link on the performance of electrical distribution networks," *Appl. Energy*, vol. 230, pp. 175-188, 2018, doi: https://doi.org/10.1016/j.apenergy.2018.08.077.

[4] D. M. Greenwood, N. S. Wade, P. C. Taylor, P. Papadopoulos, and N. Heyward, "A Probabilistic Method Combining Electrical Energy Storage and Real-Time Thermal Ratings to Defer Network Reinforcement," *IEEE Trans. Sustain. Energy*, vol. 8, no. 1, pp. 374-384, 2017, doi: 10.1109/TSTE.2016.2600320.

[5] H. Khani and H. E. Z. Farag, "Joint Arbitrage and Operating Reserve Scheduling of Energy Storage Through Optimal Adaptive Allocation of the State of Charge," *IEEE Trans. Sustain. Energy*, vol. 10, no. 4, pp. 1705-1717, 2019, doi: 10.1109/TSTE.2018.2869882.

[6] IESO. "IESO Report: Energy Storage." http://www.ieso.ca/Documents/Energy-Storage/IESO-Energy-Storage-Report_March-2016.pdf (accessed.

[7] C. Yao, C. Zhou, J. Yu, K. Xu, P. Li, and G. Song, "A Sequential Optimization Method for Soft Open Point Integrated with Energy Storage in Active Distribution Networks," *Energy Procedia*, vol. 145, pp. 528-533, 2018, doi: https://doi.org/10.1016/j.egypro.2018.04.077.

[8] S. Boyd and L. Vandenberghe, *Convex Optimization*. Cambridge University Press, 2004.

[9] A. Soroudi, P. Siano, and A. Keane, "Optimal DR and ESS Scheduling for Distribution Losses Payments Minimization Under Electricity Price Uncertainty," *IEEE Trans. Smart Grid*, vol. 7, no. 1, pp. 261-272, 2016, doi: 10.1109/TSG.2015.2453017.

[10] Evolvdso, "D1.2 Evaluation of Current Market Architectures and Regulatory Frameworks and the Role of DSOs," 2014.

[11] J. Hailin, M. Marek-Sadowska, and S. R. Nassif, "Benefits and costs of power-gating technique," in *2005 International Conference on Computer Design*, 2005, pp. 559-566, doi: 10.1109/ICCD.2005.34.

[12] J. M. Bloemink and T. C. Green, "Required VSC efficiency for zero net-loss distribution network active compensation," in *2016 IEEE 7th International Symposium on Power Electronics for Distributed Generation Systems (PEDG)*, 2016, pp. 1-8, doi: 10.1109/PEDG.2016.7527014.

[13] D. Krishnamurthy, C. Uckun, Z. Zhou, P. R. Thimmapuram, and A. Botterud, "Energy Storage Arbitrage Under Day-Ahead and Real-Time Price Uncertainty," *IEEE Trans. Power Syst.*, vol. 33, no. 1, pp. 84-93, 2018, doi: 10.1109/TPWRS.2017.2685347.

[14] M. Peker, A. S. Kocaman, and B. Y. Kara, "Benefits of transmission switching and energy storage in power systems with high renewable energy penetration," *Appl. Energy*, vol. 228, pp. 1182-1197, 2018, doi: https://doi.org/10.1016/j.apenergy.2018.07.008.

[15] M. Peker, A. S. Kocaman, and B. Y. Kara, "A two-stage stochastic programming approach for reliability constrained power system expansion planning," *Int. J. Elect. Power Energy Syst.*, vol. 103, pp. 458-469, 2018, doi: https://doi.org/10.1016/j.ijepes.2018.06.013.

[16] J. Wang, N. Zhou, and Q. Wang, "Data-driven stochastic service restoration in unbalanced active distribution networks with multi-terminal soft open points," *Int. J. Elect. Power Energy Syst.*, vol. 121, p. 106069, 2020, doi: https://doi.org/10.1016/j.ijepes.2020.106069.

[17] D. Huo, C. Gu, D. Greenwood, Z. Wang, P. Zhao, and J. Li, "Chance-constrained optimization for integrated local energy systems operation considering correlated wind generation," *Int. J. Elect. Power Energy Syst.*, vol. 132, p. 107153, 2021, doi: https://doi.org/10.1016/j.ijepes.2021.107153.

[18] D. Bertsimas, E. Litvinov, X. A. Sun, J. Zhao, and T. Zheng, "Adaptive Robust Optimization for the Security Constrained Unit Commitment Problem," *IEEE Trans. Power Syst.*, vol. 28, no. 1, pp. 52-63, 2013, doi: 10.1109/TPWRS.2012.2205021.

[19] B. Zeng and L. Zhao, "Solving two-stage robust optimization problems using a column-and-constraint generation method," *Oper. Res. Lett.*, vol. 41, no. 5, pp. 457-461, 2013, doi: https://doi.org/10.1016/j.orl.2013.05.003.

[20] A. Ben-Tal, L. E. Ghaoui, and A. Nemirovski, *Robust Optimization* (Princeton Series in Applied Mathematics). 2009.

[21] T. Sayfutdinov, C. Patsios, D. Greenwood, M. Peker, and I. Sarantakos, "Optimization-based modelling and game-theoretic framework for techno-economic analysis of demand-side flexibility: a real case study," *arXiv preprint arXiv:2110.07285*, 2021.

[22] M. Lubin, "Mixed-integer convex optimization: outer approximation algorithms and modeling power," PhD Thesis, Massachusetts Institute of Technology, USA, 2017.

[23] R. A. Jabr, R. Singh, and B. C. Pal, "Minimum Loss Network Reconfiguration Using Mixed-Integer Convex Programming," *IEEE Trans. Power Syst.*, vol. 27, no. 2, pp. 1106-1115, 2012, doi: 10.1109/TPWRS.2011.2180406.

[24] M. Braun, "Provision of ancillary services by distributed generators: Technological and economic perspective," PhD Thesis, University of Kassel, Germany, 2009.

[25] H. Akagi, T. Yamagishi, N. M. L. Tan, S. Kinouchi, Y. Miyazaki, and M. Koyama, "Power-Loss Breakdown of a 750-V 100-kW 20-kHz Bidirectional Isolated DC–DC Converter Using SiC-MOSFET/SBD Dual Modules," *IEEE Trans. Ind. Appl.*, vol. 51, no. 1, pp. 420-428, 2015, doi: 10.1109/TIA.2014.2331426.

[26] M. H. Bierhoff and F. W. Fuchs, "Semiconductor losses in voltage source and current source IGBT converters based on analytical derivation," in

2004 IEEE 35th Annual Power Electronics Specialists Conference, 2004, doi: 10.1109/PESC.2004.1355283.

[27] C. Patsios *et al.*, "An integrated approach for the analysis and control of grid connected energy storage systems," *J. Energy Storage*, vol. 5, pp. 48-61, 2016, doi: https://doi.org/10.1016/j.est.2015.11.011.

[28] British Standards Institution, "BS EN 62751-1:2014+A1:2018, Power losses in voltage sourced converter (VSC) valves for high-voltage direct current (HVDC) systems," 2018.

[29] British Standards Institution, "BS EN IEC 61803:2020, Determination of power losses in high-voltage direct current (HVDC) converter stations with line-commutated converters," 2020.

[30] A. A. Akhil *et al.*, "DOE/EPRI Electricity Storage Handbook in Collaboration with NRECA," Sandia National Laboratories, 2015.

[31] F. M. Gatta, A. Geri, S. Lauria, M. Maccioni, and F. Palone, "Battery energy storage efficiency calculation including auxiliary losses: Technology comparison and operating strategies," in *2015 IEEE Eindhoven PowerTech*, 2015, doi: 10.1109/PTC.2015.7232464.

[32] J. W. Kolar, J. Biela, S. Waffler, T. Friedli, and U. Badstuebner, "Performance trends and limitations of power electronic systems," in *2010 6th International Conference on Integrated Power Electronics Systems*, 2010.

[33] A. Blinov, R. Kosenko, A. Chub, and D. Vinnikov, "Bidirectional soft-switching dc–dc converter for battery energy storage systems," *IET Power Electron.*, vol. 11, no. 12, pp. 2000-2009, 2018, doi: https://doi.org/10.1049/iet-pel.2018.5054.

[34] M. Koller, T. Borsche, A. Ulbig, and G. Andersson, "Review of grid applications with the Zurich 1MW battery energy storage system," *Elect. Power Syst. Res.*, vol. 120, pp. 128-135, 2015, doi: https://doi.org/10.1016/j.epsr.2014.06.023.

[35] M. E. Baran and F. F. Wu, "Network reconfiguration in distribution systems for loss reduction and load balancing," *IEEE Trans. Power Del.*, vol. 4, no. 2, pp. 1401-1407, Apr. 1989, doi: 10.1109/61.25627.

[36] M. E. Baran and F. F. Wu, "Optimal capacitor placement on radial distribution systems," *IEEE Trans. Power Del.*, vol. 4, no. 1, pp. 725-734, 1989, doi: 10.1109/61.19265.

[37] M. Farivar, C. R. Clarke, S. H. Low, and K. M. Chandy, "Inverter VAR control for distribution systems with renewables," in *2011 IEEE International Conference on Smart Grid Communications (SmartGridComm)*, 2011, pp. 457-462, doi: 10.1109/SmartGridComm.2011.6102366.

[38] M. Farivar and S. H. Low, "Branch Flow Model: Relaxations and Convexification—Part I," *IEEE Trans. Power Syst.*, vol. 28, no. 3, pp. 2554-2564, 2013, doi: 10.1109/TPWRS.2013.2255317.

[39] I. Sarantakos, N. M. Zografou-Barredo, D. Huo, and D. Greenwood, "A Reliability-Based Method to Quantify the Capacity Value of Soft Open Points in Distribution Networks," *IEEE Trans. Power Syst.*, vol. 36, no. 6, pp. 5032-5043, 2021, doi: 10.1109/TPWRS.2021.3071088.

[40] A. Gholami, T. Shekari, and S. Grijalva, "Proactive Management of Microgrids for Resiliency Enhancement: An Adaptive Robust Approach," *IEEE Trans. Sustain. Energy*, vol. 10, no. 1, pp. 470-480, 2019, doi: 10.1109/TSTE.2017.2740433.

[41] J. F. Benders, "Partitioning procedures for solving mixed-variables programming problems," *Numer. Math.*, vol. 4, no. 1, pp. 238-252, 1962, doi: 10.1007/BF01386316.

[42] A. M. Geoffrion, "Generalized Benders decomposition," *J. Optim. Theory Appl.*, vol. 10, no. 4, pp. 237-260, 1972, doi: 10.1007/BF00934810.

[43] R. A. Jabr, "Robust Transmission Network Expansion Planning With Uncertain Renewable Generation and Loads," *IEEE Trans. Power Syst.*, vol. 28, no. 4, pp. 4558-4567, 2013, doi: 10.1109/TPWRS.2013.2267058.

[44] A. Ben-Tal and A. Nemirovski, *Lectures on Modern Convex Optimization*. Philadelphia, PA, USA: SIAM, 2001.

[45] MOSEK ApS. "MOSEK Modeling Cookbook." https://docs.mosek.com/MOSEKModelingCookbook.pdf (accessed.

[46] Elexon. "Load Profiles." https://www.elexon.co.uk/operations-settlement/profiling/ (accessed.

[47] "Renewables.ninja." https://www.renewables.ninja/ (accessed.

[48] Elexon. "Price Profiles." https://www.bmreports.com/bmrs/?q=balancing/marketindex (accessed.

[49] J. Lofberg, "YALMIP : a toolbox for modeling and optimization in MATLAB," in *2004 IEEE International Conference on Robotics and Automation*, 2004, pp. 284-289, doi: 10.1109/CACSD.2004.1393890.

[50] Gurobi Optimization LLC. "Gurobi Optimizer Reference Manual." http://www.gurobi.com (accessed.

[51] N. M. Zografou-Barredo, C. Patsios, I. Sarantakos, P. Davison, S. L. Walker, and P. C. Taylor, "MicroGrid Resilience-Oriented Scheduling: A Robust MISOCP Model," *IEEE Trans. Smart Grid*, vol. 12, no. 3, pp. 1867-1879, 2021, doi: 10.1109/TSG.2020.3039713.

[52] K. Chen, W. Wu, B. Zhang, S. Djokic, and G. P. Harrison, "A Method to Evaluate Total Supply Capability of Distribution Systems Considering Network Reconfiguration and Daily Load Curves," *IEEE Trans. Power Syst.*, vol. 31, no. 3, pp. 2096-2104, 2016, doi: 10.1109/TPWRS.2015.2444792.

[53] D. Bertsimas and M. Sim, "The Price of Robustness," *Oper. Res.*, vol. 52, no. 1, pp. 35-53, 2004, doi: 10.1287/opre.1030.0065.

[54] D. Greenwood, I. Sarantakos, P. Davison, C. Patsios, A. Ahmad, and M. Black, "Enhancing the Understanding of Distribution Network Losses," in *25th Int. Conf. Exhibition on Electricity Distribution (CIRED)*, Madrid, Spain, 2019, doi: http://dx.doi.org/10.34890/458.

[55] I. Sarantakos, D. Greenwood, P. Davison, and C. Patsios, "Enhanced Understanding of Network Losses: Network Modelling and Initial Results," National Centre for Energy Systems Integration (CESI), Newcastle University, 2019. [Online]. Available: https://www.northernpowergrid.com/asset/0/document/5461.pdf

[56] I. Sarantakos, D. Greenwood, P. Davison, and C. Patsios. *Real-World Distribution Network and Loading Data*, Newcastle University. [Online]. Available: https://data.ncl.ac.uk/articles/dataset/Real-World_Distribution_Network_and_Loading_Data/16456014

[57] W. Cao, J. Wu, N. Jenkins, C. Wang, and T. Green, "Benefits analysis of Soft Open Points for electrical distribution network operation," *Appl. Energy*, vol. 165, pp. 36-47, Mar. 2016, doi: https://doi.org/10.1016/j.apenergy.2015.12.022.

Ilias Sarantakos received the Dipl. Ing. degree from the School of Electrical and Computer Engineering, National Technical University of Athens, Greece, in 2013, and the Ph.D. degree from the School of Engineering, Newcastle University, UK, in 2019. Since 2018 he has been a Postdoctoral Researcher with the Electrical Power Research Group, Newcastle University. His research interests include distribution network operation and planning, optimization, reliability, and security of supply.

Meltem Peker received the M.S. and Ph.D. degrees from the Department of Industrial Engineering at Bilkent University in 2013 and 2019, respectively. She is currently a postdoctoral researcher with the Electrical Power Research Group, Newcastle University. Her research interests include energy infrastructure design, optimization and modelling of energy systems, and electricity market design.

Natalia-Maria Zografou-Barredo received the Diploma degree from the Department of Electrical and Computer Engineering, School of Engineering, University of Patras, Greece in 2016, and completed her Ph.D. research in electrical and electronic engineering at the School of Engineering, Newcastle University, U.K. in 2021. She is an EPSRC Doctoral Prize Fellow in the School of Engineering, at Newcastle University, U.K. Her research interests include distribution network operation, active network management, and mathematical optimization. She is the recipient of the 2016 IEEE Greece Power and Energy Society POWERED Award (16th Workshop on Power Engineering Dissertations).

Matthew Deakin (M'19) received the M. Eng degree in Engineering Science in 2015 from the University of Oxford, U.K., for which he was awarded the Lubbock prize. He then held a Clarendon Scholarship for the duration of his PhD in Engineering Science, which was awarded by the University of Oxford in 2020. Since 2019 he has been a Research Associate at Newcastle University. His research interests include hybrid AC/DC networks, the integration of low carbon technologies, and whole energy systems.

Charalampos (Haris) Patsios is a Senior Lecturer in Power Systems in the School of Engineering at Newcastle University. He has significant experience in the design, modelling and control of electrical power systems including Energy Storage, Renewables and Power Electronics. His research involves the development of models, grid interfaces and control techniques for energy storage systems as well as decentralized asset scheduling and planning in future power networks, working closely with UK industry and academia. He has attracted relevant research funding exceeding £2.1m in personal split from Industry and Research Councils, leading as principal investigator in 14 grants.

Timur Sayfutdinov received his Ph.D. degree in Engineering from Skolkovo Institute of Science and Technology (Russia) in 2020. Currently, he is working as a Research Associate at the School of Engineering of Newcastle University (UK). His research involves the development of models and control algorithms for electricity network assets (including storage and demand-side flexibility) and the development of behavioral models of stakeholders for multi-agent modelling of the future network scenarios.

Phil C. Taylor (Senior Member, IEEE) was appointed as the Pro Vice-Chancellor for Research and Enterprise with the University of Bristol, Bristol, U.K., in summer 2020. He was with industry and academia of energy systems for more than 25 years. In 2013, he joined Newcastle University, Newcastle upon Tyne, U.K., as the Dean and Director of the multidisciplinary Institute for Sustainability, and later, became the Head of the School of Engineering. He is currently Co-Director of the £20m EPSRC National Centre for Energy Systems Integration and also the Director of the £10m EPSRC Supergen Energy Networks Hub, which brings together industrial and academic partners including five UK universities with other energy network stakeholders. He was with industry including GEC Alstom, EPS (UK), Teradyne, and Senergy Econnect. He is a Member of the Board of Trustees for National Energy Action, a fuel poverty charity. In addition to being a Visiting Professor with Nanyang Technological University, Singapore, he is also a nonexecutive Director of Northern Powergrid, an electrical distribution company, which provides power to eight million customers in the North East and Yorkshire.

David Greenwood (M'14) received the M.Eng. degree in new and renewable energy from Durham University, Durham, U.K., in 2010 and the Ph.D. degree, for work on real-rime thermal ratings, from Newcastle University, Newcastle upon Tyne, U.K., in 2014. He is a Newcastle University Academic Track Fellow focussing on whole systems approaches to energy.